JOURNAL OF MULTIFUNCTIONAL MATERIALS & PHOTOSCIENCE
9(2), December 2018, pp. 209-239

Inorganic Semiconductors-graphene Nanocomposites as a Counter Electrode for Dye-sensitized Solar Cells (DSSC) Applications : Review

Yonrapach Areerob [b] and Won-Chun Oh[a,b*]**

[a] *College of Materials Science and Engineering, Anhui University of Science & Technology, Huainan 232001, PR China*
[b] *Department of Advanced Materials Science & Engineering, Hanseo University, Chungnam 356-706, South Korea*

Abstract: Graphene materials consisting of a single atomic layer of graphite have wide potential applications in electronic, optoelectronic, and energy storage devices due to their remarkable electrical, optical, and tunable band gap properties. Dye-sensitized solar cells (DSSCs) which offer high photo-to-electric conversion efficiencies at low production cost have attracted a great deal of interest. Application of graphene materials into each part DSSC component, including photoanode, electrolyte and cathode has been recently well developed. This review will focus on recent advances in graphene and their application as materials to improve the photovoltaic performance of DSSCs.

1. Introduction

Dye-sensitized solar cells (DSSCs) have attracted both academic and industrial interests as promising low-cost solar cells because of their relatively high photo-to-electric conversion efficiencies, low production cost, and environmental benignity [1,2]. Fig. 1 depicts the structure and components of a traditional DSSCs, which usually comprises photoanode, electrolyte and cathode [3]. In 2014, a conversion efficiency as high as 13% had been achieved based on a porphyrin dye in liquid electrolyte DSSCs [4]. However, some technological and scientific difficulties, such as maximizing light harvesting, minimizing losses during the electron transfer pathways, and (or) leakage (or) evaporation of the organic liquid electrolyte, still need to be resolved before the applications of DSSCs become practical [5,6].

In order to improve the photovoltaic performance and lower the cost of DSSCs, incorporation of new materials has been considered. For instance, organic dyes have been synthesized and applied to replace the rare metal-containing dyes [7]. Meanwhile, solid-state hole conductors, poly (ionic liquids) and ionic plastic crystals with high ionic

* Corresponding author*: wc_oh@hanseo.ac.kr; yonrapach@gmail.com*

conductivities, have also been invented to replace the traditional organic liquid electrolytes [8–12]. In addition, transition metal compounds, conducting polymers, and carbon materials have been introduced as alternative catalysts to platinum in the cathode [13–16].

Among the materials pursued to improve the performance of DSSCs, graphene, a type of two-dimensional carbon material, has been explored, due to graphene's unique properties. These include high carrier mobility, excellent transmittance, and large specific surface area. For example, monolayer graphene has a high carrier mobility (>200 000 cm^{-2} V^{-1} s^{-1} at an electron density of 4 $\times 10^9$ cm^{-2}), high specific surface area (2600 m^{-2} g^{-1}), and high optical transparency (97.7%). All these advantages allow graphene to be a promising material for efficient and practical DSSCs [17–21].

Graphene materials were first used as transparent electrodes in 2008 to replace fluorine doped tin oxide (FTO) at the photoanode [22]. With increasing depth of research, many other advantages of graphene materials were discovered, such as harvesting light, increasing ion transport through both the TiO_2 layer and the electrolyte, and replacing platinum at the cathode [23–24]. The unique properties and general applications of graphene materials have been reviewed by Neto, [25] Geim [26] and more recently by Xu [27]. This review focuses on recent applications of graphene materials in photoanode, electrolyte and cathode sections of DSSCs (see Fig. 1).

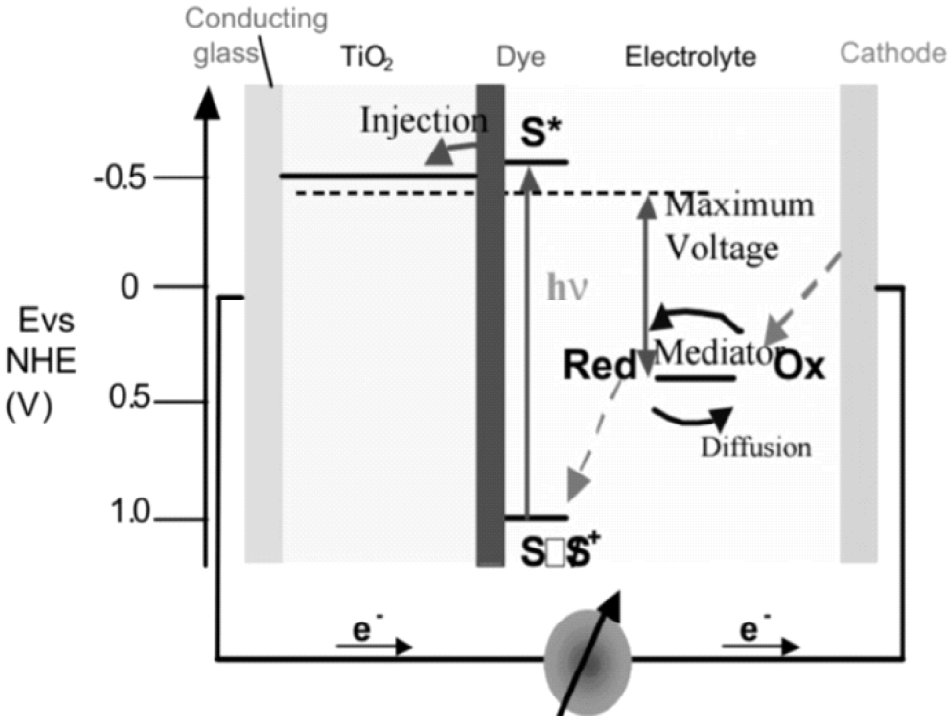

Figure 1: Operating principles of dye-sensitized solar cells. Reprinted with permission from ref. [3].

Heterogeneous photocatalysis based on the utilization of semi- conductors such as TiO_2 [28–33], CuO [34,35], ZnO [36,37], and Fe_2O_3 [38–40] to produce highly reactive radical species able to trigger oxidative reactions, as well as conduction band (CB) electrons promoting reduction conversions, presents many advantages, including low operation cost and no production of secondary hazardous metabolites. The open challenges before photocatalytic processes become economically feasible for large scale industrial applications include the need to enhance efficiency under solar radiation, and to mitigate recombination of photogenerated electrons and holes. Several strategies have been developed including doping with metal and non-metal species, coupling with other semiconductors, and sensitization with organic chromophores [5, 25–31], which have not all yet resulted in practical applications.

The discovery of GR [41], a 2D form allotrope of carbon and zero band gap semiconductor [42] exhibiting extraordinary electron mobility (106 m s^{-1}), excellent large surface area (2630 m^2 g^{-1}) responsible for improved interfacial contact with other species [43], and high chemical stability and mechanical resistance [44–46], might soon solve many of the practical problems encountered in photocatalysis [47], especially now that economically feasible synthetic routes to GR are becoming available [48].

GR has different physicochemical features depending on the synthesis technique used for its preparation: bottom-up, where the smallest building blocks of the material are assembled together to obtain a high quality GR [28,39–41] and top-down by breaking down graphite into the desired material by chemical or physical processes (Fig. 2) [42–46]. The latter approach opened up the possibility of massive production when solution-based chemistry was discovered [47].

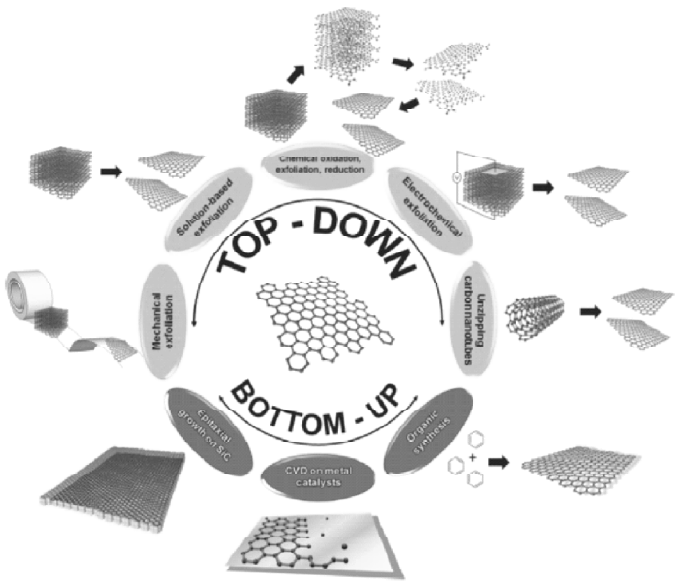

Figure 2: Routes for the synthesis of GR. Reprinted with permission from Ref. [39]. Copyright 2014 American Chemical Society.

Early applications of GR in photocatalysis mostly relied on reduced graphene oxide (RGO) [45,48], rather than on GR, obtained via thermal [49], chemical [46], and electrochemical [39], reduction of graphene oxide (GO) synthesized by modified Hummer methods [42,50]. The presence of covalently bonded oxygenated groups (including hydroxyl, epoxy, carboxyl etc.) in the GO structure offered anchoring points for the binding of semiconductors. Structural defects and abundance of oxygen bearing groups in the GO structure, however, impact on electrical properties by interrupting the conductive delocalized-conjugation and also induce a tendency to aggregate with a final detrimental effect not only on specific surface area, but also on electronic properties [37,47,51–53].

In general, GR-semiconductor composites form photocatalysts showing enhanced activity toward pollutants abatement, photoreduction of CO_2 and photocatalytic hydrogen evolution, thanks to i) the suppressed recombination of photogenerated electrons and holes, ii) extended absorption range of light wavelengths, and iii) better adsorption of reactants [54–57]. Furthermore, these characteristics can be tuned and optimized working on many factors including tunable layer number, edge morphology, crystallinity degree, type and extent of defects, size effect and exposed crystal facets [37,58–65].

In this account, we address the challenges and opportunities in the production of second generation GR-semiconductor composites. Recent advances in the synthesis and photo(electro)catalytic applications, and in the understanding of the interaction mechanisms among different moieties in the resulting nanostructures are discussed and put in context with the aim to provide guide- lines in the development of new composites capable of meeting productivity, stability and cost requirements needed for practical application in the emerging solar [66] and bio-based [67] economy. Throughout the described applications, a special consideration is given to the ability of GR to provide a platform to attract and convey electrons, promote (photo)adsorption of reacting substrates, and enlarge the absorption range of semiconductors towards the visible region [37,56,68].

2. Synthetic techniques

In the fabrication of GR semiconductor composites, GR behaves either as compositing component of inorganic semiconductors, or as a substrate where the semiconductors are grown/supported. A number of methods do exist allowing for the fabrication of GR-semiconductors composites with diverse morphology, size, dimensionality and interfacial domains [69], all affecting the efficiency of the photocatalytic processes. However, all the synthetic techniques producing GR conjugated composites can be categorized into: in situ crystallization and ex-situ hybridization [70].

In situ crystallization, which is the most common method, is based on the direct and homogenous growth of nanomaterials (such as nanoparticles, nanowires, nanorods, nanotubes or nanofilms) on the surface of a GR precursor, mainly GO or RGO [70]. In situ crystallization is based on mixing GO or RGO and the soluble precursors of the inorganic semiconductors in a solvent, following a chemical, thermal, optical or ultrasonic treatment of the mixture to finally anchor the inorganic catalysts on the surface of GR. The oxygen sites of GO act as nucleation points for the adjustment of size, morphology and crystallinity

of the nanoparticles and enable the efficient interfacial contact of nanomaterials on GO/RGO surface to improve the efficiency of electron transfer. In situ methods including sol-gel method, hydrothermal/solvothermal treatment, and microwave-assisted deposition have been exploited to fabricate GR based composites through a one-step growth or by a multi-step reaction procedure.

Sol-gel method, a wet chemical approach, is based on phase transition from a precursor, a colloidal liquid, into a solid gel through a series of hydrolysis and polycondensation reactions. Its key advantage is the effective anchoring of the catalyst at the OH groups of GO/RGO by chemical bonding. The precursors used in the preparation of GR-semiconductor composites are mostly metal alkoxides, metal chlorides, and organometallic compounds. As an example, in the fabrication of TiO_2-RGO or GO composite photocatalysts via a sol-gel method, the precursors used were titanium tetraisopropoxide (TTIP) [71–73], titanium butoxide (TBOT) [26,74–77], and titanium tetrachloride ($TiCl_4$) [78], which resulted in different structures of TiO2 depending on the experimental conditions applied. From TTIP the following steps produced a composite catalyst:

$$GO_xH_y + (CH(CH_3)_2O_4Ti \xrightarrow{O_2,C_3H_7OH,\text{unbalanced}} \{(CH(CH_3)_2\text{-}O)_3Ti\text{-}O\}\text{-}G+CH(CH_3)_2\text{-}OH \quad (1)$$

Final drying and annealing at temperatures typically above 300°C resulted in semiconductor photocatalysts, whose crystallinity and photocatalytic activity were strongly affected by the final heat treatment. Studies on the structural integrity of GR- inorganic semiconductor composites have been conducted by Chun et al. [79], who found out that a high temperature up to 400°C in the final treatment enhances the photocatalytic activity of TiO 2-3% (w/w) GO without significantly affecting its structural features. Hydrothermal/solvothermal method is widely used for the fabrication of composite photocatalysts, based on crystallization of catalysts on GO sheets with the simultaneous reduction of GO at high temperature and pressure. It can take place with or without reductants starting from an aqueous/alcoholic solution [80–83]. Sher Shah *et al.* [84] synthesized Ag-TiO_2-RGO, a ternary nanocomposite photocatalyst, by dispersing TTIP in N,N dimethyl- formamide (DMF) and ethylene glycol (EG) containing silver nitrate and RGO to reduce silver nitrate to silver and mitigate the agglomeration of RGO nanosheets upon treatment at 200 °C for 18 h, as illustrated in Fig. 3. The resulting Ag and TiO_2 nanoparticles were evenly distributed on RGO sheets without agglomeration of RGO. During the fabrication of GR-semiconductor photocatalysts, Liu *et al.* [85] targeted different exposed facets of TiO_2, namely {101}, {100}, and {001}, to be grown on GR through a hydrothermal reaction by capping anions at 180 °C for 24 h. After a thorough structural and physicochemical analysis, they reported that directionality on the facet growth also affected the photocatalytic activity by changing the bonding structure of GR and TiO_2, and thus the interfacial charge transfer rates.

Microwave-assisted synthesis is a fast and low temperature method of producing GR-inorganic semiconductors composites compared to other in situ procedures. This technique enables to induce nucleation and growth of small and homogenous particles on GR [86].

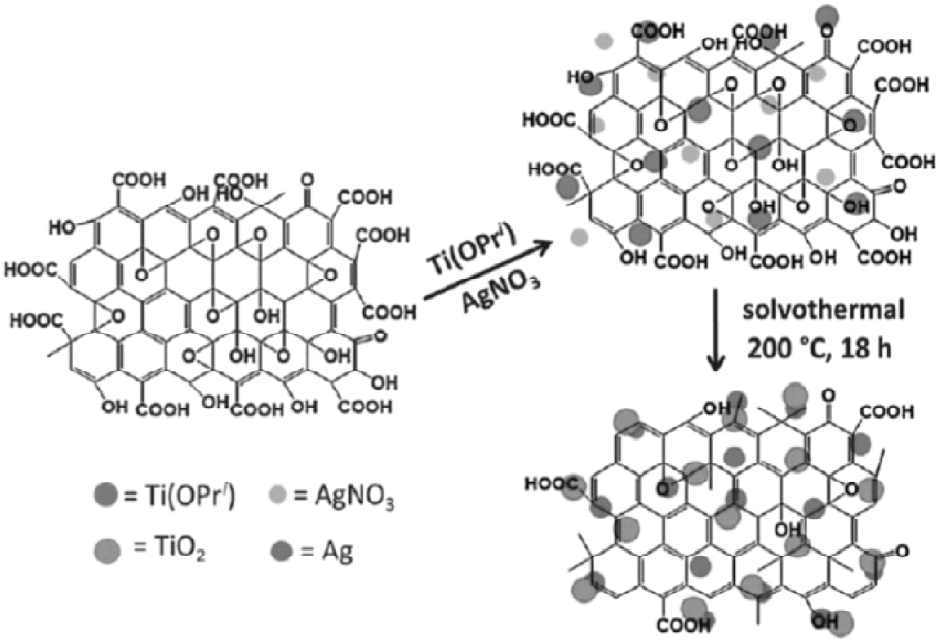

Figure 3: Fabrication of Ag-TiO_2-RGO ternary nanocomposite photocatalyst. Reprinted with permission from Ref. [84]. Copyright 2013 Royal Society of Chemistry.

UV microwave-assisted technique was used during the fabrication of OH-TiO_2/RGO by UV irradiation of their precursors, i.e. TBOT and GO, and treating them through microwaves [59]. The results indicated that surface hydroxylation on RGO/TiO_2 catalyst enabled extension of visible light absorption up to about 600 nm with a color shift to yellow, at the same time reducing crystal sizes, inducing surface defects such as Ti^{3+} states and oxygen vacancies, thereby enhancing charge transfer with a lower recombination rate.

All reviewed studies on in situ synthesis suggest that GO is the most used precursor of GR because of its high degree of hydrophilic functional groups that allows for water processability. TiO_2 and CdS also seem to have made the forefront of inorganic semiconductors that are mostly composited with GR. TiO_2-GR composites seem to be commonplace because of TiO_2 availability, nontoxicity and economic favorability. TiO_2 precursors used include TTIP, TBOT and $TiCl_4$; with the choice of precursor and synthetic method being dependent on the structures and morphology of the required composites. Among the in situ methods, microwave-assisted synthesis is fast compared to sol-gel and hydrothermal. However, hydrothermal treatment seems to be the most widely used because GO is fairly reduced to RGO, thus yielding a better photocatalytic activity of the resulting composite materials.

Ex-situ hybridization is based on mixing nanomaterials with a defined structure and composition with GR precursors, aiming to anchor the inorganic particles to oxygen moieties existing at the surface of GO or RGO via covalent or noncovalent interaction

[70]. For instance, coating GO sheets on a Nb-doped TiO_2 (TNO) thin film resulted in a transparent conducting oxide (TCO) layer fabricated by a self-assembly technique, and being indium free, low cost and enhancing charge transport. According to the photocatalytic activity measurement, GO on TNO films exhibit an improved photocatalytic efficiency on degradation of methylene blue (MB) [55].

In self-assembly technique, the distribution of nanomaterial on GR is random. For this reason, to maximize unique properties of GR, the surface modification of either GR or the inorganic semiconductors is necessary to improve their ability to process solvent, and to increase the spatial interaction between GR and the catalysts [54]. Xiao *et al.* [87] constructed 2% RGO/SiO_2 hollow microsphere composites via ultrasound-assisted interfacial self-assembling of negatively charged GO sheets on positively charged SiO_2 modified with poly(diallyldimethylammonium) chloride (PDDA). Sonication enabled the composite to disperse in the aqueous solution thus preventing aggregation. The following solvothermal treat- ment resulted in a further reduction of GO and better interfacial contact between SiO_2 and RGO.

Another approach involves the aerosol assisted self-assembly method, which is simple, low cost and easy to scale up, allowing to achieve a charge transfer between TiO_2 and RGO sheets and to foster interfacial contact between TiO_2 and RGO compared to the electrostatic assembly approach [88]. From the perspective of synthesizing composites with robust interfacial contact between inorganic catalysts and GR, the ex- situ synthesis method is often less efficient than in situ. The stronger interfacial interactions can be attributed to the generation of chemical bonds which tends to foster the effective separation of electron-hole pairs with an efficient electron transfer and the narrowing of optical band gaps. Conversely, we want to highlight that the advantage of ex-situ method is to the control of the morphology of the materials into ordered and monodisperse structures by pre-selection of semiconductors with desirable morphology. In the course of ex-situ preparations, the shape, size and morphology of the used semiconductors in the composites are nearly the same as the initial ones. A fair comparison of the photoactivity of the composites with respect to inorganic semiconductors is then feasible, without any concern on the morphological structure influence.

3. Dimensionality of composites

Besides doping/codoping techniques to modulate the carrier separation and transfer of GR-semiconductor, several studies indicated that the photocatalytic performance of GR-semiconductor composites are also improved by tuning surface area, mass transfer kinetics and local assembly environment, since these parameters have a synergistic effect on the whole photocatalytic reactions. We can differentiate among quantum dots, which are zero-dimensional (0D), nanoribbons, nanotubes, nanowires and nanorods, belonging to the one-dimensional (1D) category, single- atom thick material like sheets being two-dimensional (2D) and, finally, nanospheres and nanocones, which are among the 3D morphologies. Dimensionality can explain the atomic assembly of the materials and also affect their properties to a significant degree. The same component can exhibit a very

different photocatalytic activity when existing in different shapes, due to a different charge mobility and reduced recombination resulting in a prolonged charge life and shorter transfer paths.

3.1. Two-dimensional structures

The dimensionality of each component of a composite and the increased interfacial contact area are able to enhance the electron transfer thus result in a better photocatalytic activity. Coupling of lower dimensional structures and GR such as in 0D/2D, 1D/2D and 2D/2D heterostructures, is an effective way for boosting the global photocatalytic performance [89]. In 0D/2D and 1D/2D composites, nanoparticles, nanorods, nanowires or nanotubes have been coupled with GR through in situ growth methods or ex-situ assembly. However, 2D/2D heterostructures have better interfacial contact areas due to the more efficient face-to-face contact, which enhances the photocatalytic performance by increasing the electron transfer and separation of photogenerated electron-hole pair compared to 0D/2D, where inorganic semiconductors are dispersed on 2D GR sheets, either homogeneously or wrapped inside nanosheets, and also compared to 1D/2D configurations, where a line-to-line interaction occurs as shown in Fig. 4 [89]. A 2D/2D arrangement has been described for instance by Luan et al. [90], who indicated that the usage of 2D TiO_2 nanosheets in the fabrication of GR-modified semiconductor catalysts has advantages, serving as a hosting material to load guest functional nanomaterials, providing a large interaction area between

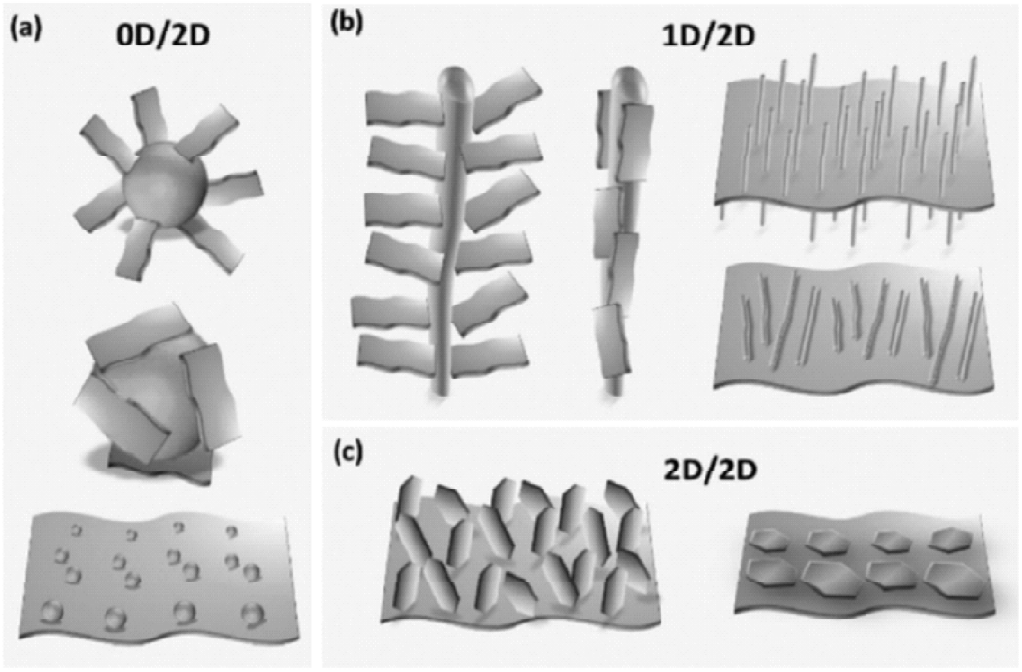

Figure 4: GR based composites with different dimensionality and interfacial contacts. Reprinted with permission from Ref. [89]. Copyright 2016 Royal Society of Chemistry.

catalyst and organic pollutant.

As reported by Bera *et al.* [91], GR/CdS nanosheets composite (2D/2D) enhances the photocatalytic activity in the degradation of MB of about 4 times, compared to GR/CdS nanorod (2D/1D), which in turn shows ca. 3.4 times greater activity than GR/CdS nanopar- ticles (2D/0D), fabricated by hydrothermal treatment. This study highlights how increasing dimensionality results in a better photocatalytic activity.

3.2. Three-dimensional structure

GR, with its unique 2D structure, can be used as the building block for the self-assembly of 3D functional materials. Due to the strong interaction among GR sheets, it is hard to dissolve GR in most solvents. However, in a gel medium, it can be well dispersed thanks to the covalent – stacking interactions with a gelator peptide [92]. Moreover, when synthesized by Hummer method, GO is soluble in water yielding a homogenous liquid which is beneficial for the 3D self-assembly procedures, producing organogels, aerogels, and hydrogels. The 3D structures obtained, for instance, in porous films, aerogels, and scaffolds, allow GR to enhance specific surface area, charge carrier transfer and conductivity, and to inhibit aggregation, by means of combination of 3D porous structure and the peculiar properties of GR, namely high surface area, high conductivity and electron mobility.

Among the several 3D structures of GR which have been reported, GR hydrogels/ aerogels have attracted widespread attention due to (i) the porous structure providing an ideal support to fabricate photocatalytic semiconductors, (ii) the shapes, volumes and densities adaptability, allowing for high adsorption ability, and (iii) the affordable and convenient recycling of the photocatalysts due to the prompt separation from the reaction media. As an example, a study focused on construction of 3D porous aerogel constituted by GR sheets and Bi_2WO_6 nanosheets, indicated that the bi-component photocatalyst achieved higher degradation of rhodamine B (RhB) compared to bare Bi_2WO_6, due to a 60% higher specific surface area and higher adsorption of RhB compared to bare Bi_2WO_6 sheets [93]. GO/polymer hybrid microspheres were fabricated by getting 2D GO sheets wrapped on the surface of polymer microspheres and assembled into 3D structures [94]. The wrinkled surface of the photocatalyst increased the specific surface area and allowed the particles to grow on 3D structures by providing effective sites [95]. The photocatalytic activity of TiO_2/RGO/polymer composites on the degradation of RhB under visible light was about 96% in 30 min, much better compared to TiO_2 Degussa P25, owing to the good crystallinity and the small size of anatase TiO_2 particles, the unique electrical conductivity of GR, and the interactions between TiO_2 and RGO in this complex composite. As a final remark on 3D assembled composites, GR functionalized by melamine resin monomer (MRGO), assembled with CdS, was reported to give an enhanced separation efficiency of photo-generated electrons by means of multidimensional transport pathways compared to CdS-RGO sheets (Fig. 5) [96].

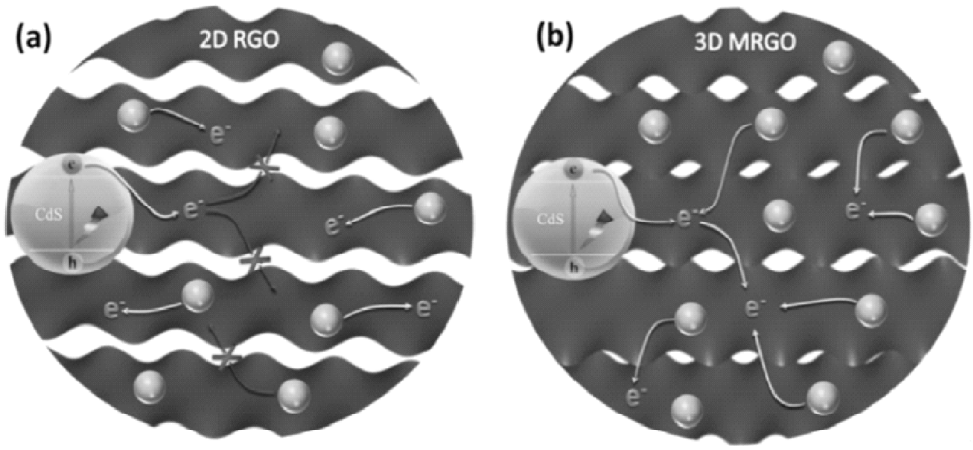

Figure 5: Schematic illustrating the charge transfer mechanism at interfaces of 3D CdS-MRGO and 2D CdS-RGO. Reprinted with permission from Ref. [96]. Copyright 2015 American Chemical Society.

Furthermore, hydroxyl end groups of melamine resin monomers were found to inhibit restacking of MRGO in the composite CdS-MRGO.

4. Graphene applications in photoanode

The photoanode of a DSSC is generally composed of a dye-sensitized TiO_2 layer coated on a transparent conducting glass or plastic substrate. Recently, graphene materials have been successfully used in photo-anodes as transparent conductors, in the TiO_2 layer, as well as in the dye-sensitizer.

4.1. Transparent electrode

Indium tin oxide (ITO) is one of the most widely used transparent electrodes due to its high conductivity and high transmittance in the visible spectrum. However, ITO films are usually brittle and unstable at high temperatures (which is required for solar cell photoanode fabrication). Therefore, fluorine doped tin oxide (FTO) electrodes have been used to replace ITO electrodes in DSSCs. Compared with ITO, FTO is relatively cheaper and can bear harsh chemical and high temperature treatment up to 700 °C [97]. Similar to FTO, graphene was considered as another alternative material to overcome the cost and performance limitations of ITO due to its high electron mobility and transparency. Since each graphene layer absorbs about 2.3% of light, the light can pass through a maximum of <“5 sheets for about 90% transmittance [98]. Fig. 6 shows the transmittance of different transparent conductors.

In 2008, Wang *et al.* reported the first fabrication of transparent and conductive graphene electrodes for DSSCs [99]. The graphene films were fabricated via the exfoliation of graphite oxide and thermal reduction of the resultant platelets. The prepared graphene films exhibited a conductivity of 550 S cm^1 and a transparency of more than 70% over

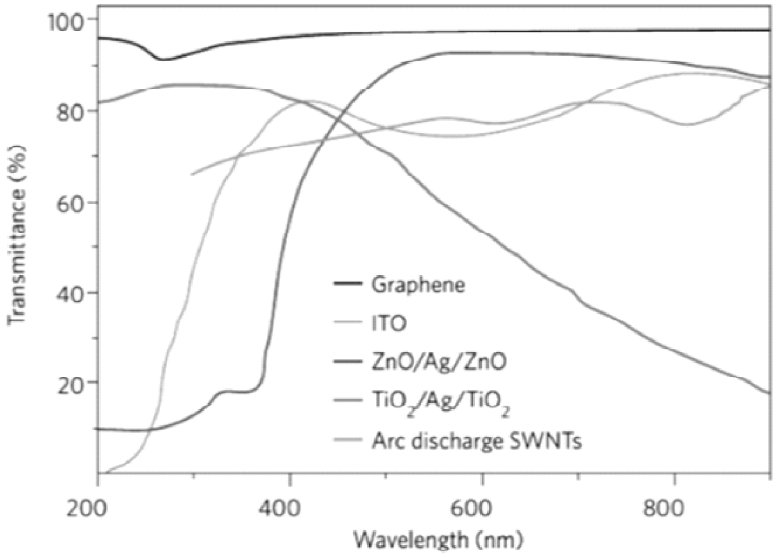

Figure 6: Transmittance for different transparent conductors: GTCFs, single-walled carbon nanotubes (SWNTs), ITO, ZnO/Ag/ZnO and TiO_2/Ag/TiO_2. Reprinted with permission from ref. [32].

the wavelength range 1000–3000 nm. After that, Huang and co- workers prepared few-layer graphene films on SiO_2 substrates via ambient pressure chemical vapor deposition. The crystal size, layer number and optical transmittance of the graphene films were tuned by Huang et al. by changing the growth time (Fig. 7). The prepared graphene films as counter electrodes of DSSCs achieved a photovoltaic efficiency of 4.25%, which is quite comparable to those of the FTO counter electrodes [100]. These results suggest the potential of graphene films for photovoltaic and electronic applications. However, there is still much work needed to be done, such as improving the scalability of the technology and effecting cost reductions.

4.2. Semiconducting layer

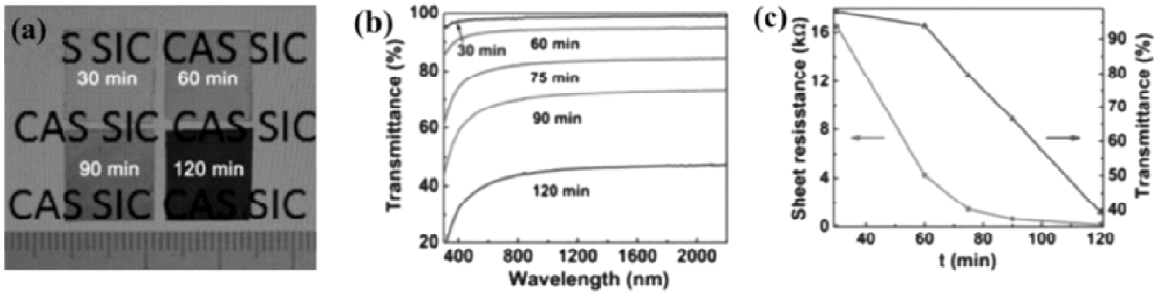

Figure 7: (a) Optical images of graphene directly grown on SiO_2 substrates at 1200 °C for the growth time of 30, 60, 90 and 120 min, respectively. (b) Optical transmittance spectra of the transferred graphene films. (c) Transmittance (at 550 nm) and sheet resistance as a function of growth time. Reprinted with permission from ref. [33].

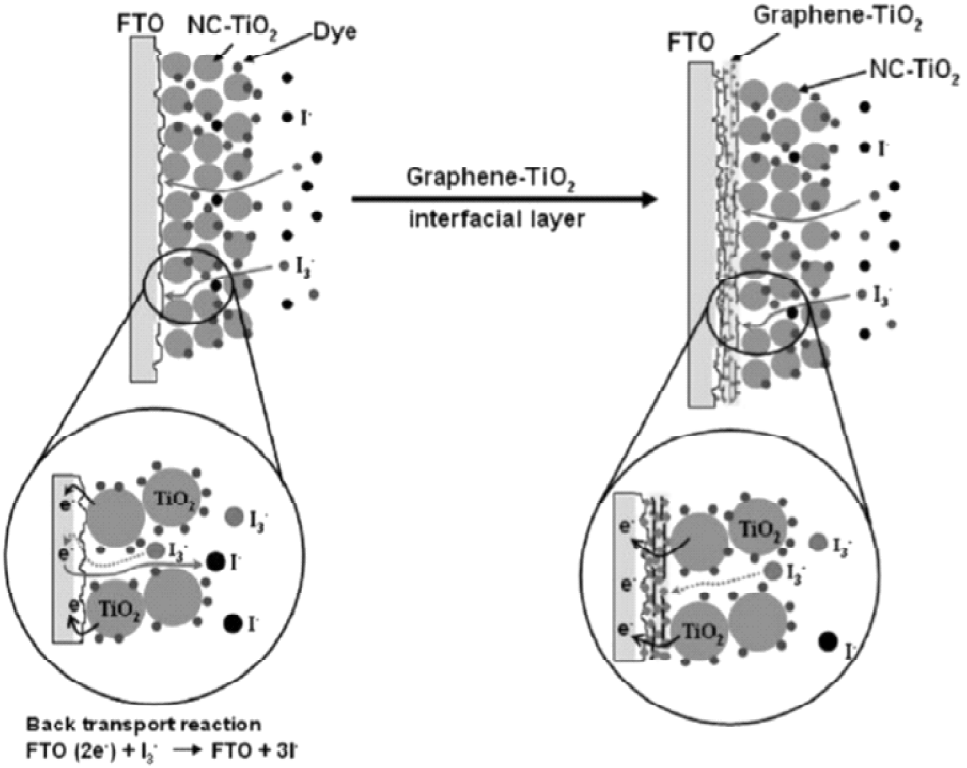

Figure 8: Schematic representation and mechanism of applied graphene–TiO_2 interfacial layer to prevent back-transport reaction of electrons. Reprinted with permission from ref. [34].

Kim *et al.* [101] reported the UV-assisted photocatalytic reduction of graphene oxide/TiO_2 nanoparticles. The prepared graphene/TiO_2 was applied as an interfacial layer between FTO and nanocrystalline (NC) TiO_2 film (see Fig. 8). Compared with a normal interfacial layer, the lower roughness of the graphene–TiO_2 interfacial layer provided better adhesion between the FTO substrate and NC-TiO_2 layer. The cell showed a power conversion efficiency (PCE) of 5.26%, which is higher than that without a blocking layer (PCE = 4.89%). However, the transmissivity decreased from 85% to 78% when compared with the traditional TiO_2 blocking layers. Chen *et al.* used a novel and efficient method to enhance the performance of the DSSCs by reducing the charge recombination process occurring at the interface of the FTO nanoparticles and the FTO/TiO_2 by spin-coating graphene on FTO [102]. The PCE of the DSSC improved dramatically from 5.80% to 8.13% mainly due to the improved charge transfer and retarded charge recombination. The blocking layer only absorbed 1.6% of light, suggesting that less than a monolayer of thermally reduced graphene oxide (TRGO) was present or that the TRGO was only slightly reduced.

The atomic thinness and high aspect ratio of graphene provide a low percolation threshold [103]. Therefore, graphene materials have also been incorporated into the

semiconducting layer to improve the performance of the DSSCs via increasing the charge collection efficiency [104, 105]. They could act as a current collector with only slight changes to TiO_2 film morphology. There are only a few reports on the use of a graphene-based current collector as a photoanode [106, 107]. Yang and co-workers were the first to begin to study this topic. The photoanode can form graphene bridges and enhance charge transport rate to prevent charge recombination and increase light collection in the device by incorporating 2D graphene into TiO_2 nanostructure [108]. On the basis of these advantages, the short-circuit current density and PCE were increased by 45% and 39%, respectively, as compared to the NC-TiO_2 photoanode. Since then, many studies focused on this area have been conducted. In these studies, it is accepted that adding graphene to the TiO_2 layer resulted in an in- crease in dye absorption, which in turn increased the light- harvesting efficiency and thereby led to an increase in photocurrent.

Although some reported results and conclusions are still inconsistent, [109,110] these studies showed the potential of obtaining high performance DSSCs. Yang *et al.* reported that the inclusion of reduced graphene oxide (RGO) induced the formation of macrospores in the scattering of TiO_2 films, which greatly increased the photocurrent of the device [111]. Fang et al. also claimed that the present of porosity was due to the voids formed from the reduction in volume of graphene oxide forming graphene during heating [112]. With increasing temperature, graphene oxide becomes dehydrated and the oxygen groups can be removed. Al- though the width of RGO is about one-half that of native graphene oxide, this change is on the nanometer scale and thus cannot be responsible for the reported light scattering, an effect that would require macroscopic porosity. Another explanation could be that including RGO in the TiO_2 scattering films affected the rheology of the paste, which prevented a smooth and dense film deposition. Durantini and co-workers [113]reported that a [solvothermally reduced graphene oxide]–TiO_2 composite absorbed 44% more light at the dyes (N719) absorption peaks (~ 370 and ~ 530 nm). This could explain the increase (~29%) in photocurrent. The results may be due to the light scattering layer; however, other optical effects such as the fact that the TRGO can act as a sensitizer could not be ruled out. Besides direct sensitization, en- hanced light harvesting could also be caused by increased absorption in the TiO_2 layer. It has been proven that the visible spectrum band gap of TiO_2 can be diminished or attenuated in the presence of graphene materials [113, 114].

Graphene materials have been incorporated into semiconductor films in a variety of ways. Park and co-workers [115] coated Al_2O_3 with graphene oxide and then mixed with TiO_2 so as to prevent sheet aggregation. Li et al. added a TRGO–YF4:Er^{3+}/Yb^{3+}composite into TiO_2 film which indicated a gradual increase in the anodic current. With an optimum content of graphene (1 wt %) doped into TiO_2 film, the PCE showed a 15% improvement from 5.98% to 6.86% [116]. In addition to the traditional TiO_2–dye in DSSCs described above, graphene materials have also been incorporated into quantum dot photochemical cells and in p-type DSSCs [117-119]. These results demonstrate that the graphene–TiO_2 composite structure effectively could increase light absorption intensity and inhibit charge recombination while enhancing charge transfer, thereby providing a promising scaffold

for quantum dots and p-type DSSCs. However, it is still unclear whether the addition of graphene materials into DSSCs would increase the performance of the DSSCs or not. For example, Neo et al. added TRGO into the TiO_2 layer. However, after a thermal treatment and further optimization, no significant increase in PCE was observed [120]. Studies on this topic are still at their initial stages; most of the explanations are based on assumptions not yet fully validated.

4.3. Sensitizer

In general, sensitizing dye has two functions: absorbing light and transferring electrons to the conduction band of the semiconductor. An efficient sensitizer should have intense absorption in the visible region (i.e. high extinction coefficient), strong adsorption affinity to the surface of the semiconductor, and stability in its oxidized form. In addition, it should have a more negative lowest unoccupied molecular orbital (LUMO) energy than the conduction band (CB) of the semiconductor and more positive highest occupied molecular orbital (HOMO) energy than the redox potential of the electrolyte [120,121].

A well-known dye, N719, is one of the most effective sensitizers for a DSSC. It absorbs wavelengths up to ~800 nm and has an extinction coefficient of ~ 1.5 × 104 $M^{-1} \cdot cm^{-1}$ at 535 nm [122]. Since graphene has a broad and strong absorption profile, absorbing about 2.3% of light with each monolayer of material, it has received interest as a possible spectral sensitizing material [123]. Recently, several groups have experimentally demonstrated that graphene materials can act as a photosensitizer [124, 125]. Zhang *et al.* fabricated a series of graphene nanocomposites as photosensitizers via a facile two-step wet chemistry method. The ZnS-RGO nanocomposites exhibit visible light photoactivity toward aerobic selective oxidation of alcohols and epoxidation of alkenes under ambient conditions. This work offers a useful guide for designing graphene-based semiconductor composite photocatalysts.

4.4. Graphene electrolyte applications

Applications of graphene in the electrolyte have been (1) as a minor additive, and (2) as a main component. The former case includes the gelation of the electrolyte and the bleaching of the electrolyte, both of which would be intriguing to try with DSSCs. Velten et al. found that when graphene nanoribbons (5.8 wt %) were added, a decrease in the optical absorption of the iodide/triiodide electrolyte was observed [58]. This phenomenon can be explained through electron transfer from the graphene nanoribbon to triiodide, resulting in a less absorbing species. Jung et al. reported that the electrolyte containing graphene sheet (~6.5 wt %) performed better than one without the TRGO [126].

A few electrolyte studies fall into the latter case, in which researchers attempted to use graphene materials in high concentrations as conductive fillers to decrease the electrolyte resistance. Ahmad et al. added a mixture of graphene and SWCNTs into 1-methyl-3-propylimidazolium iodide with the goal of improving electrolyte conductivity [127]. The graphene nanoribbon material (30 wt %) based quasi-solid state electrolytes displayed an increase of PCE from 0.16% to 2.10%. They suggested that the increase in

efficiency is attributed to the filler materials, which act as the extended electron transfer surfaces, and as catalysts for the electrochemical reduction of I^-_3 . It is noted the application of a graphene material in the electrolyte may be severely limited by the catalytic activity of graphene for the reduction of triiodide, which could effectively create a short circuit in the cell.

5. Graphene cathode applications

5.1. DSSC with graphene as a cathode

In DSSCs, the counter electrode is utilized to collect holes from the hole conducting material. The optimal cell is one that has the lowest possible sheet resistance for the counter electrode material, demonstrates excellent catalytic activity for redox electrolyte reduction, exhibits high chemical stability, and has a low production cost. Since the first work on high efficiency DSSC was published in 1991, platinum (Pt) had been frequently used as counter electrodes in conventional DSSCs. Recently alternative materials that can also act as counter electrodes have been reported [128]. One such material is graphene, which demonstrates high electrocatalytic activity and outstanding conductivity, allowing it to be a promising substitute to Pt as a counter electrode. Work from various research groups on DSSCs with graphene counter electrodes is listed in Table 2 [129-135]. The reported efficiencies of DSSCs with graphene counter electrodes vary from 0.74% to 9.4%. This variation is primarily accounted by the diverse techniques used for the graphene film preparation and the DSSC fabrication method [61,62,72]. Shi's group was the first that we know of to incorporate graphene materials as the catalytic cathode of a DSSC [67]. Preparation of graphene sheets was achieved by reducing graphene oxide (RGO), which was noncovalently functionalized with 1- pyrenebutyrate (PB^-). The resulting PB^--G was spin-coated on a FTO substrate. The efficiency of the DSSC with graphene as a cathode was found to be 2.20%, compared to the conventional DSSC using Pt that had an efficiency of 3.98%. Following this discovery, a series of studies has been published, analyzing how the degree of reduction affects catalytic performance. [61,73–76]

Graphene nanoplatelets (GNP), as a basic morphology of graphene, have been used as the counter electrode material, due to its higher active sites, i.e. edge defects and oxidic groups [136]. In the I^-_3/I^- redox reaction, electrocatalytic properties of GNP are proportional to the concentration of active sites and are independent of the electrolyte medium. In an ionic liquid (Z952) based electrolyte, GNP demonstrated high electrocatalytic activity toward the I^-_3/I^- redox couple [137]. When compared to the traditional electrolyte based on methoxypropionitrile solution (Z946), Z952 ionic liquid had a charge transfer resistance (Rct) values smaller by a factor of 5–6. It has been proved that thermal annealing is an efficient way to further lower the Rct as reported in various works [61,73, 74]; while the doping is another widely reported method [138]. To date, the highest DSSC efficiency (9.4%) was obtained using GNP based counter electrodes from Gratzel's group [139]. High electrocatalytic activity for the $Co(bpy)^{3+/2+}$ redox couple in acetonitrile electrolyte solution

Table 1
DSSC performance of devices with graphene materials in the TiO_2 layer compared to control cells

Sample	*Graphene content (wt %)*	*Jsc (mA/cm^2)*	*Voc (V)*	*η (%)*	*Ref.*
Underlayer with T-CRGO	0.04	6.7	0.56	1.7	[38]
Scaffold layer with T-CRGO	0.6	16.3	0.69	7.0	[36]
Scaffold with thermally treated CTAB-functionalized graphene	0.5	12.8	0.82	6.5	[25]
Scaffold layer with TRGO	0.83	7.6	0.67	2.8	[37]
Scaffold layer with CVD-derived graphene on Al2O3	1	10.2	0.78	5.4	[39]
Scaffold layer with unknown graphene material	1	19.9	0.70	6.9	[40]
Scaffold layer with T-CRGO	1	8.4	0.75	4.3	[41]
Scaffold layer with CRGO	0.5	12.9	0.68	6.1	[42]
Underlayer with RGO, scaffold layer with RGO, scattering layer with RGO	1	23.2	0.73	9.2	[43]

Table 2
PV characteristics of DSSC enabled by graphene counter electrode

Sample	*Jsc (mA/cm^2)*	*Voc (V)*	*η (%)*	*Ref.*
GNP	17.0	0.75	6.8	[61]
Graphene	7.7	0.68	2.8	[62]
Graphene	6.12	0.64	2.19	[63]
Graphene	8.1	0.72	2.6	[64]
Graphene	6.4	0.70	0.74	[65]
Graphene	12.9	0.70	4.7	[66]
Pyrenebutyrate-functionalized graphene	13.6	0.55	2.2	[67]
Porous graphene	12.2	0.71	5.20	[68]
CF4 functionalized graphene	10.9	0.66	2.6	[69]

is exhibited in GNP. Compared to the traditional electrocatalyst, or platinum, the GNP film is superior in charge-transfer resistance (exchange current) and as well as electrochemical stability under prolonged potential cy- cling. GNP's effective electrochemical performance allows the material to act as the redox shuttle for DSSCs with Y123-sensitized TiO_2 photoanodes and $Co(bpy)^{3+/2+}$. In comparison to the DSSC with the Pt-FTO cathode, the DSSC with the GNP cathode is preferable in both fill factor and in power conversion efficiency at higher illumination intensity. Grinding RGO and then thermolyzing the composite to achieve the high porosity were reported, but the performance (7.2%) was still lower than that of the traditional DSSC (7.8%)

[140]. A chemical vapor de- position (CVD)-derived graphene structure with the average pore size of 40–50 nm, was reported. Spacer materials, such as SiO_2 particles and some residue was also used to increase SA by keeping graphene apart [141]. The performance of their novel DSSC (5.0%) is close to that of the DSSC with Pt (5.5%).

Two main approaches to further improve the performance of graphene in the DSSC system were taken: Firstly, improving morphology to increase the surface area in general, [27,65,68,78–80] and secondly chemically modifying the material to increase the material's intrinsic activity [69,81,82]. Morphology and the micro-structure have attracted much attention, in which three types of graphene sheets were investigated: 1) Thicker graphene film, [142] horizontal oriented graphene nanosheets, and vertically oriented nanosheets were used in DSSC fabrication [143]. Vertical orientation graphene nanosheets showed the best DSSC performance, indicating that assessable surface area and ion mobility were higher in the DSSC. 2) The use of porous graphene was also an efficient way to create high assessable surface area. Porous structures could offer higher surface area, which should improve the performance of counter electrodes as the catalyst by mitigating redox recombination. The efficiency of DSSC with porous graphene achieved a PCE value of 5.2%, which was reported by Jang's group [144]. Secondly, to increase intrinsic activity, chemically doped graphene, such as nitrogen-doped graphene [69,81, 82,87] and CF4 functionalized graphene and HNO_3 treated graphene, was also used as the counter electrode in the DSSC. In addition to the DSSC with the traditional I_3 /I electrolyte, it is evident that graphene can perform differently in other electrolyte systems, such as cobalt-based and sulfur-based mediators.

5.2. DSSCs with graphene/carbon nanotube cathodes

Carbon nanotubes (CNTs), including single-walled carbon nanotubes (SWCNTs), few-walled carbon nanotubes (FWCNTs), and multiwalled carbon nanotubes (MWCNTs), have been well investigated as catalytic materials for DSSCs [88–94]. This interest in SWCNTs and MWCNTs is attributed to their remarkable electrical conductivity and extremely large and tunable surface areas. Additionally, the ability to control their defect edges could allow facilitation of the electron kinetics associated with I_3 reduction. Furthermore, graphene's demonstrated potential for counter electrode application, as previously discussed, has led to the recent interest in exploring graphene/CNT composites in this capacity (Table 3) [95–100].

Table 3
PV characteristics of DSSC enabled by graphene/CNTs counter electrode

Counter electrode	*Jsc (mA/cm²)*	*Voc (V)*	*η (%)*	*Ref.*
Graphene/MWCNTs	5.6	0.75	3.00	[95]
Graphene/MWCNTs	9.0	0.72	4.46	[96]
Reduced Graphene/MWCNTs	12.9	0.78	6.2	[97]
Graphene/MWCNTs	8.8	0.77	4.0	[98]
Graphene/FWCNTs	16.1	0.75	7.6	[99]

Choi and co-workers [95] synthesized a graphene/MWCNTs composite material counter electrode by growing carbon nanotubes on chemically reduced graphene layers through CVD. They were able to achieve greater energy conversion efficiency, namely 3%, with this ma- terial. The cell exhibited higher energy conversion efficiency than that of the DSSC with a MWCNTs based counter electrode. What accounts for this greater efficiency is the expansion of the reaction area (at the interface) due to the vertically grown MWCNTs on the graphene sheets. To further improve the performance of graphene/MWCNTs counter electrodes, the preparation method was modified by first preparing graphene on a SiO_2/Si substrate via CVD followed by growing carbon nanotubes on top of the graphene layer [145]. Using this preparation method, the DSSC with the CVD graphene/MWCNTs counter electrode showed a cell efficiency of 4.46%; a substantial increase from the previously mentioned 3.0%.

Other groups have additionally prepared graphene/CNTs composite materials using different methods and reported various cell efficiencies. Using the electrophoretic deposition method, Zhu et al. synthesized reduced graphene/CNTs composite materials as DSSC counter electrodes [146]. Battumer et al. prepared graphene/CNTs composite films with the doctor blade method and further confirmed the optimized composition of CNTs in the graphene/CNTs composite counter electrode of 60% [147]. The formation of a graphene-CNTs network structure allowed an initial increase in DSSC efficiency. However, the final decrease in efficiency may be caused by the lower specific surface area of CNTs when compared to that of graphene sheets [148]. In addition, Velten et al. reported that the DSSC graphene/MWCNTs composite counter electrode, at an efficiency of 7.55%, had a higher power conversion efficiency than that of the DSSC with MWCNTs alone, whose efficiency was 6.62% [149]. The increase in electrical conductivity between the MWCNT bundles and the graphene sheets allows for a greater efficiency as demonstrated in the DSSC with a graphene/MWCNTs composite counter electrode. [150]

Another material, recently found by Lou's group that can act as a novel DSSC cathode is flexible, seamlessly covalently bonded, three- dimensional vertically aligned few-walled carbon nanotubes (VAFWCNTs)/graphene on metal foil formed in to a transparent conducting oxide with Pt [151]. This new VAFWCNTs/graphene on metal foil combination is promising as an inexpensive, high- performing, flexible cathode for solar cell application. The schematic images of the cathode and the novel DSSC are shown in Fig. 9. Compared to the traditional combination in a brittle Pt/fluorine-doped tin oxide cathode, this VAFWCNTs/graphene cathode has a lower charge transfer resistance and lower contact resistance between the catalyst and the substrate. The covalent bonds of graphene and VAFWCNTs allow exceptional electron transport through the electrode. Additionally, the large surface area of the hybrid carbon materials enables catalytic capability rivaling that of the Pt analogue. In both rigid and flexible assemblies, DSSCs utilizing this flexible VAFWCNTs/graphene hybrid cathode surpassed the performance of Pt-based cells. This VAFWCNTs/graphene hybrid cathode operated at 8.2% in rigid assemblies, whereas the Pt- based cell performed at 6.4%. Similarly, the hybrid carbon cathode performed at 3.9% in flexible assemblies, in comparison to 3.4% for the Pt- based cell.

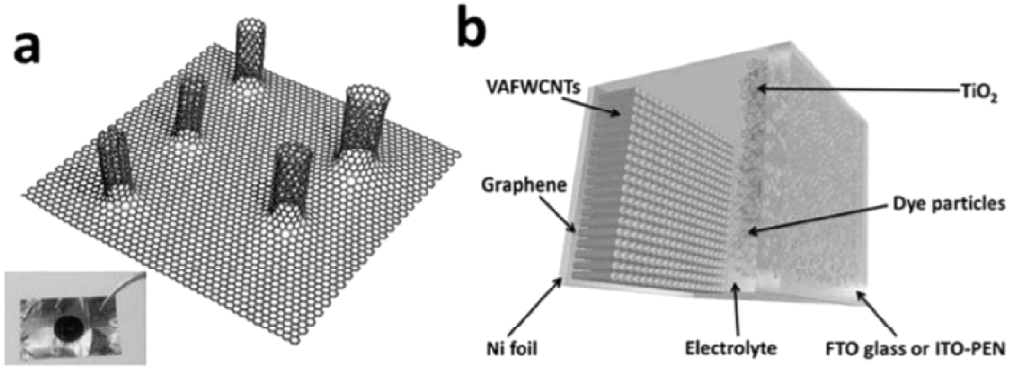

Figure 9: Schematic image of the novel DSSCs. (a) Schematic structure of the VAFWCNTs/graphene as the counter electrode. The inset image represents the VAFWCNTs/graphene (black circle) on the Ni foil as the counter electrode. (b) Schematic image of the novel DSSC. Reprinted with permission from ref. [100].

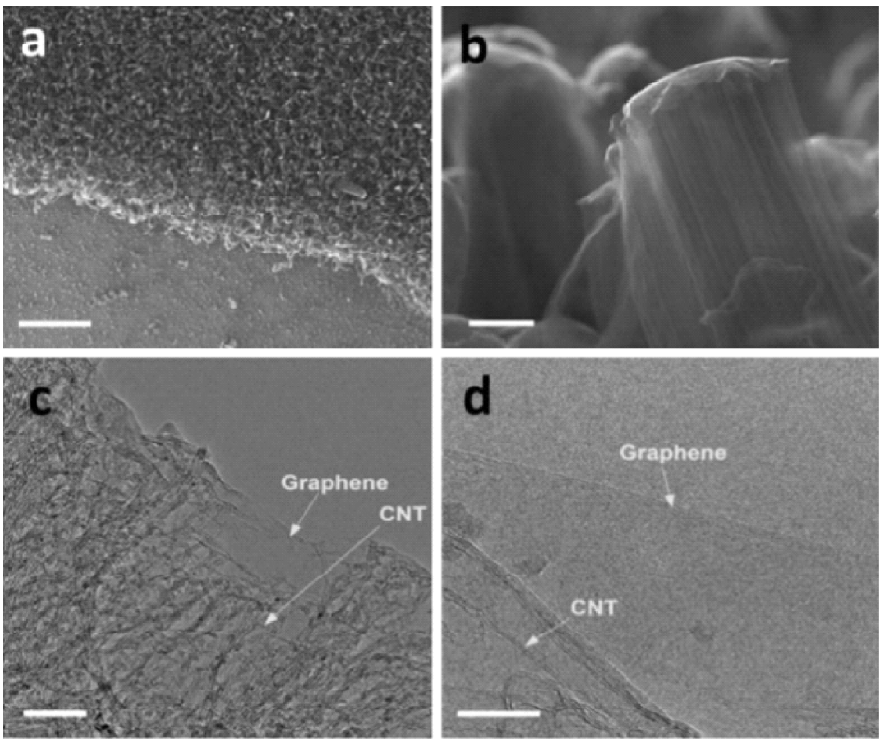

Figure 10: Characterization of the cathode materials. (a) Top view SEM image of the VAFWCNTs/graphene on Ni foil, scale bar = 50 mm. (b) Side view SEM image of the VAFWCNTs/graphene on Ni foil with high magnification, scale bar = 2 mm. (c) TEM image showing that the CNT forest is connected to the graphene film. Scale bar = 100 nm. (d) High-resolution TEM image showing that the graphene is few-layered and the CNTs materials are one- to three-walled, scale bar = 10 nm. Reprinted with permission from ref. [100].

A top view of the edge of the CNTs forest on a graphene-covered Ni substrate is shown in Fig. 10a. The SEM image of the VAFWCNTs sections (Fig. 10b) reflects the tip-growth mechanism. The graphene layer is vital for preventing catalyst aggregation during growth, which allows an increased growth rate of the VAFWCNTs on the metal substrate. Fig. 10c and d show a fused structure that is formed from the graphene and CNTs after growth.

Experimental results show that the CNTs/graphene/Ni material may be an ideal high-performance, flexible, and cost-effective alternative cathode for DSSCs, as shown in Fig. 11. For the semi-rigid DSSC, the EIS analysis showed that the new cathode only had a resistance of 0.91 Ω, which is more than 20 times lower than that of the Pt cathode (19.6 Ω), thus leading to a much higher electron transfer rate at the cathode/electrolyte interface. Additionally, truly flexible DSSCs are able to be synthesized with the flexible properties of the CNTs/ graphene/Ni electrode. These flexible DSSCs demonstrate a PCE of 3.9%, compared to the Pt cathode that has a PCE of 3.4%. The reason for the higher electrocatalytic activity in the flexible DSSCs may be the combination of the high surface area of the hybrid electrode and the seamless electrical connection between the VAFWCNTs and the graphene layer.

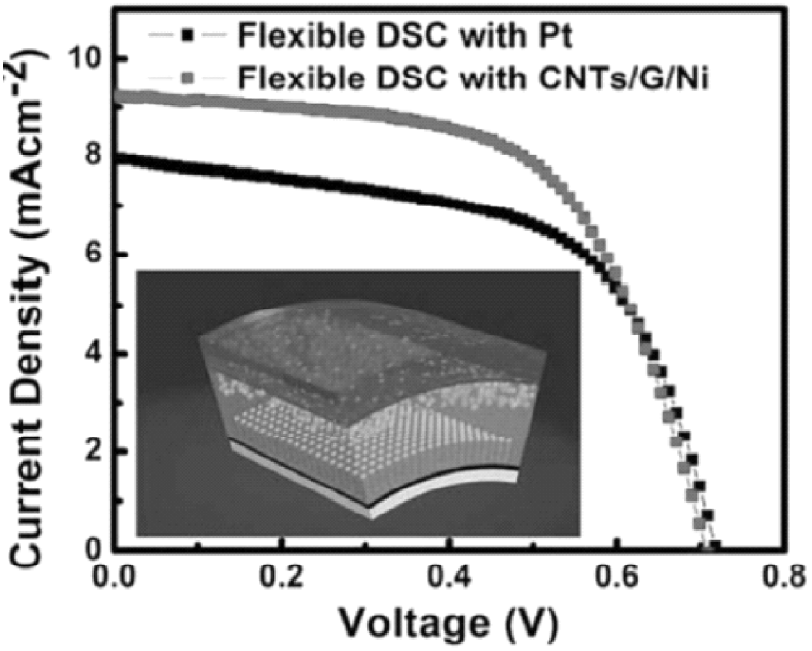

Figure 11: Photocurrent–voltage characteristics of flexible DSSCs using CNTs/G/Ni or Pt as the cathode under 1 Sun illumination (AM 1.5 G, 100 mW cm^{-2}). The inset is a schematic diagram of the flexible DSSC. Reprinted with permission from ref. [100].

5.3. DSSCs with graphene/metal as cathode

Another material being investigated is a Pt/graphene composite material. The use of Pt/graphene composite materials as counter electrodes are one approach to reduce Pt loading in DSSCs, as shown in Table 4 [66,101–103]. This should lead to a much smaller production cost for the DSSC. Using the self-assembly of polyelectrolyte, graphene, and H_2PtCl_6, followed by an annealing treatment, Gong *et al*. fabricated a Pt/graphene composite [152]. Additionally, the Pt/graphene composite based cell reached a power conversion efficiency of 7.66%, comparable to that of the sputtered-Pt based cell at 8.16%. Bajai *et al* further investigated the effect of Pt loading on the PV performance of the DSSCs by depositing Pt nanoparticles on graphene layers using a pulsed laser ablation method. They found that the amount of Pt loading had a remarkable impact on DSSC efficiency [153]. The group obtained an optimized Pt loading of 27.43% and reported that not only did the DSSC with the optimized Pt/graphene counter electrode contain a lower amount of Pt, but also exhibited higher energy conversion efficiency. The improved efficiency was attributed to the increase in the graphene sheet defects, caused by increased Pt deposition into the graphene sheets [154].

As an alternative to Pt, Ni was combined with graphene, forming composite counter electrodes in other studies. Dou et al. embedded $Ni_{12}P_5$ nanoparticles into graphene sheets using a hydrothermal reaction to synthesize the $Ni_{12}P_5$/graphene composites [66]. The $Ni_{12}P_5$/graphene demonstrated excellent electrocatalytic activity for I_3 reduction, resulting in a high efficiency of 5.7% for this DSSC as shown in Table 4. Graphene's role in these metal/graphene composite materials was that of a well dispersed metal (Pt or $Ni_{12}P_5$) particle scaffold, increasing the availability of the metal particles for electron transfer [66,103]. Furthermore, graphene improved the rate of electron transfer at the interface by providing a fast diffusion pathway for the electrolyte and allowing excellent electrode–electrolyte contact. The metal (Pt or $Ni_{12}P_5$) nanoparticle can act as the active site for electrocatalytic processes as well as the spacer between the graphene sheets, and therefore accelerate the diffusion.

Table 4
PV characteristics of DSSC enabled by graphene/metal counter electrode

Counter electrode	*Jsc (mA/cm²)*	*Voc (V)*	*η (%)*	*Ref.*
Graphene/$Ni_{12}P_5$	12.86	0.74	5.70	[66]
Graphene	12.88	0.70	4.70	[101]
Graphene/Pt	15.20	0.71	7.66	[102]
Graphene/Pt	6.67	0.74	2.90	[103]
Graphene/Pt	12.06	0.79	6.35	[105]

4.4. DSSCs with graphene/polymer as cathode

Graphene/conductive polymer composite films have recently served as counter electrodes in DSSCs, as listed in Table 5 [27,62,81,97, 104–110]. In these composite films, the polymer, i.e. polystyrene sulfonate doped poly(3,4-ethylenedioxythiophene) (PEDOT-PSS) enables

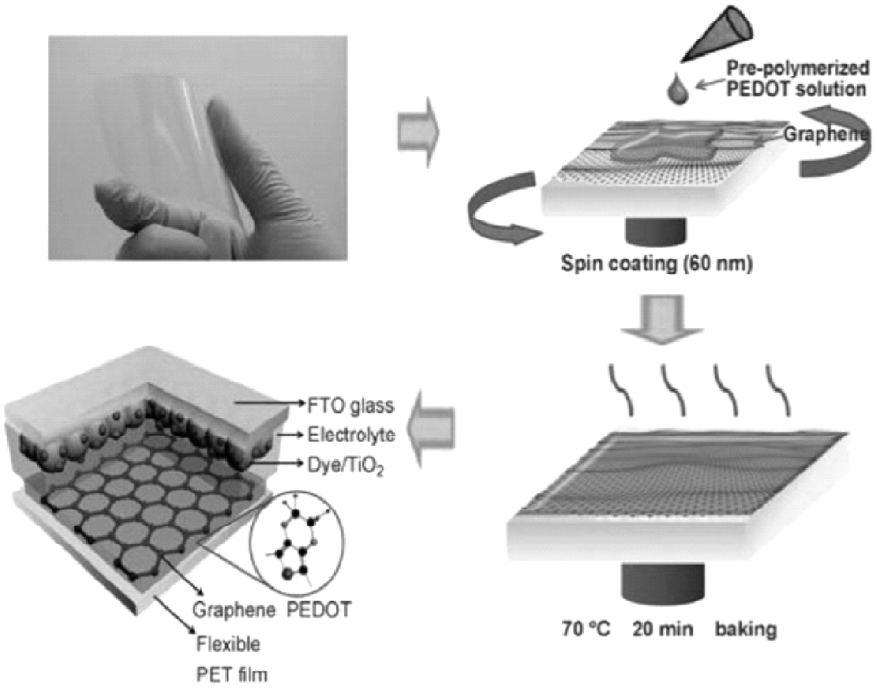

Figure 12: Photograph of a graphene-coated PET substrate, and schematic diagram of the fabrication steps involved in preparing a DSSC with a graphene/PEDOT counter electrode on a PET substrate. Reprinted with permission from ref. [106].

conductivity, while the graphene enables catalysis [104]. The DSSC with such a graphene/PEDOT-PSS counter electrode had an efficiency of 4.5%, outperforming the DSSC with a PEDOT-PSS counter electrode without graphene, whose efficiency was 2.3% [104]. As an alternative to being dispersed in the polymer matrix, [104] graphene can addition- ally serve as the polymer's support [105]. Furthermore, Park's group reported of a DSSC with the graphene/PEDOT composite counter electrode exhibiting a high efficiency of 6.26%, due to the presence of graphene in PEDOT. Graphene-incorporated PEDOT results not only in exceptional electrochemical activity, but also in much more rapid trans- port through the composite film [106]. The schematic image is shown in Fig. 12.

6. Conclusion

As a rising star in material science, graphene has been recently used as one of the key components of DSSCs demonstrating high performance characteristics. Considering the photoanode, it is believed that proper addition of graphene might, in certain cases, improve the photo- current in some cases. However, it is still not clear whether a selectively and carefully graphene doped photoanode would increase the PCE of the devices. As a sensitizer, graphene show advantages in multiple carrier generation and hot injection,

and provide a possible way to over- come the inherent limit of current device structures. Appropriate concentration (minor additive) of various graphene in the electrolyte may improve the performance of DSSCs, However, high concentration of graphene will decrease the performance of the device due to their catalytic activity and high light absorptions. At the cathode materials, the excellent catalytic activity for the reduction of the redox reaction positions graphene and its composites to be a strong candidate for replacing both Pt and FTO in cathodes for DSSC. Based on the reported results, it is clear that graphene materials will have wide and important future applications in DSSCs. However, it should be noted that applications of graphene materials in DSSCs are still at their initial stages. Most of mechanisms discussed are based on various untested assumptions. Various graphene materials with different properties should be extensively studied as different components before the significant and practical application of graphene materials to DSSCs is realized.

Reference

[1] F. Meneguzzo, R. Ciriminna, L. Albanese, M. Pagliaro, The energy-population conundrum and its possible solution, ArXiv. org (2016).

[2] Y. Areerob, J.Y. Cho, W.K. Jang, K.Y. Cho, W.C. Oh , An alternative of NiCoSe doped graphene hybrid $La_6W_2O_{15}$ for renewable energy conversion used in dye-sensitized solar cells, Solid state Ionic 327 (2018) 99-109.

[3] F. Parrino, G. Camera-Roda, V. Loddo, G. Palmisano, V. Augugliaro, Combination of ozonation and photocatalysis for purification of aqueous effluents containing formic acid as probe pollutant and bromide ion, Water Res. 50 (2014) 189–199.

[4] W.C. Oh, K.Y. Cho, C.H. Jung, Y.Areerob, Three-dimensional of graphene oxide Ba_2VPbSe_6 framework composite attach on cellulose based counter electrode for dye-sensitized Solar cell, J. Photochem. Photobiol., A 372 (2019) 11–20.

[5] C.H. Ao, S.C. Lee, Indoor air purification by photocatalyst TiO_2 immobilized on an activated carbon filter installed in an air cleaner, Chem. Eng. Sci. 60 (2005) 103–109.

[6] Y. Areerob, K.Y. Cho, C.H. Jung, W.C. Oh, Synergetic effect of $La_2CdSnTiO_4$-WSe_2 perovskite structured nanoparticles on graphene oxide for high efficiency of dye sensitized solar cells, J Alloys Compd 775 (2019) 690-697.

[7] Y. Yamazaki, H. Takeda, O. Ishitani, Photocatalytic reduction of CO_2 using metal complexes, J. Photochem. Photobiol. C Photochem. Rev. 25 (2015) 106–137.

[8] K. Li, X. An, K.H. Park, M. Khraisheh, J. Tang, A critical review of CO2 photoconversion: catalysts and reactors, Catal. Today 224 (2014) 3–12.

[9] Y. Areerob, K.Y. Cho, W.C. Oh, Microwave assisted synthesis of graphene-$Bi_8La_{10}O_{27}$ nanocomposite as efficient catalytic counter electrode for dye- sensitized solar cell, New J. Chem. 41 (2017) 9613-9622.

[10] Y. Ma, X. Wang, Y. Jia, X. Chen, H. Han, C. Li, Titanium dioxide-based nanomaterials for photocatalytic fuel generations, Chem. Rev. 114 (2014) 9987–10043.

[11] N.S. Chaudhari, S.S. Warule, S.A. Dhanmane, M.V. Kulkarni, M. Valant, B.B. Kale, Nanostructured N-doped TiO_2 marigold flowers for an efficient solar hydrogen production from H_2S, Nanoscale 5 (2013) 9383–9390.

[12] S.M. El-Sheikh, T.M. Khedr, A. Hakki, A.A. Ismail, W.A. Badawy, D.W. Bahnemann, Visible light activated carbon and nitrogen co-doped mesoporous TiO_2 as efficient photocatalyst for degradation of ibuprofen, Sep. Purif. Technol. 173 (2017) 258–268.

[13] X.H. Lin, Y. Wu, J. Xiang, D. He, S.F.Y. Li, Elucidation of mesopore-organic molecules interactions in mesoporous TiO_2 photocatalysts to improve photocatalytic activity, Appl. Catal. B 199 (2016) 64–74.

[14] S. Yang, L. Gao, Photocatalytic activity of nitrogen doped rutile TiO_2 nanoparticles under visible light irradiation, Mater. Res. Bull. 43 (2008) 1872–1876.

[15] G. Kumordzi, G. Malekshoar, E.K. Yanful, A.K. Ray, Solar photocatalytic degradation of Zn^{2+} using graphene based TiO_2 , Sep. Purif. Technol. 168 (2016) 294–301.

[16] V. Augugliaro, M. Bellardita, V. Loddo, G. Palmisano, L. Palmisano, S. Yurdakal, Overview on oxidation mechanisms of organic compounds by TiO_2 in heterogeneous photocatalysis, J. Photochem. Photobiol. C Photochem. Rev. 13 (2012) 224–245.

[17] Q. Zhang, K. Zhang, D. Xu, G. Yang, H. Huang, F. Nie, C. Liu, S. Yang, CuO nanostructures: synthesis, characterization, growth mechanisms, fundamental properties, and applications, Prog. Mater. Sci. 60 (2014) 208–337.

[18] X. Liu, J. Chen, P. Liu, H. Zhang, G. Li, T. An, H. Zhao, Controlled growth of CuO/Cu_2 O hollow microsphere composites as efficient visible-light-active photocatalysts, Appl. Catal. A 521 (2016) 34–41.

[19] D. Sudha, P. Sivakumar, Review on the photocatalytic activity of various composite catalysts, Chem. Eng. Process. Process Intensif. 97 (2015) 112–133.

[20] M. Shekofteh-Gohari, A. Habibi-Yangjeh, Fabrication of novel magnetically separable visible-light-driven photocatalysts through photosensitization of Fe_3O_4/ZnO with $CuWO_4$, J. Ind. Eng. Chem. 44 (2016) 174–184.

[21] W.-J. Liu, F.-X. Zeng, H. Jiang, X.-S. Zhang, W.-W. Li, Composite Fe_2O_3 and ZrO_2/Al_2O_3 photocatalyst: preparation, characterization, and studies on the photocatalytic activity and chemical stability, Chem. Eng. J. 180 (2012) 9–18.

[22] O. Mehraj, B.M. Pirzada, N.A. Mir, M.Z. Khan, S. Sabir, A highly efficient visible-light-driven novel p-n junction Fe_2O_3/BiOI photocatalyst: surface decoration of BiOI nanosheets with Fe2 O3 nanoparticles, Appl. Surf. Sci. 387 (2016) 642–651.

[23] Z. Wei, X. Wei, S. Wang, D. He, Preparation and visible-light photocatalytic activity of Fe_2O_3/ Fe_2O_3magnetic heterophase photocatalyst, Mater. Lett. 118 (2014) 107–110.

[24] M. Pagliaro, R. Ciriminna, G. Palmisano, Silica-based hybrid coatings, J. Mater. Chem. 19 (2009) 3116–3126.

[25] X. Pan, M.-Q. Yang, Z.-R. Tang, Y.-J. Xu, Noncovalently functionalized graphene-directed synthesis of ultralarge graphene-based TiO_2 nanosheet composites: tunable morphology and photocatalytic applications, J. Phys. Chem. C. 118 (2014) 27325–27335.

[26] H.-H. Chun, J.Y. Lee, J.-H. Lee, W.-K. Jo, Enhanced photocatalysis of graphene and TiO2 dual-coupled carbon nanofibers post-treated at various temperatures, Ind. Eng. Chem. Res. 55 (2016) 45–53.

[27] N. Liu, L. Fu, B. Dai, K. Yan, X. Liu, R. Zhao, Y. Zhang, Z. Liu, Universal segregation growth approach to wafer-size graphene from non-noble metals, Nano Lett. 11 (2011) 297–303.

[28] C. Garlisi, G. Scandura, J. Szlachetko, S. Ahmadi, J. Sa, G. Palmisano, E-beam evaporated TiO2 and Cu-TiO2 on glass: performance in the discoloration of methylene blue and 2-propanol oxidation, Appl. Catal. A 526 (2016) 191–199.

[29] B.S. Tek, S. Yurdakal, L. Ozcan, V. Augugliaro, V. Loddo, G. Palmisano, N-doped anatase/rutile photocatalysts for the synthesis of aromatic aldehydes under ultraviolet and solar Irradiation, Sci. Adv. Mater. 7 (2015) 2306–2319.

[30] C. Guarisco, G. Palmisano, G. Calogero, R. Ciriminna, G. Di Marco, V. Loddo, M. Pagliaro, F. Parrino, Visible-light driven oxidation of gaseous aliphatic alcohols to the corresponding carbonyls via TiO2 sensitized by a perylene derivative, Environ. Sci. Pollut. Res. 21 (2014) 11135–11141.

[31] K.S. Novoselov, A.K. Geim, S.V. Morozov, D. Jiang, Y. Zhang, S.V. Dubonos, I.V. Grigorieva, A.A. Firsov, Electric field effect in atomically thin carbon films, Science 306 (2004) 666–669.

[32] C. Lee, X. Wei, J.W. Kysar, J. Hone, Measurement of the elastic properties and intrinsic strength of monolayer graphene, Science 321 (2008) 385–388.

[33] A.A. Balandin, S. Ghosh, W. Bao, I. Calizo, D. Teweldebrhan, F. Miao, C.N. Lau, Superior thermal conductivity of single-layer graphene, Nano Lett. 8 (2008) 902–907.

[34] L. Liu, M. Qing, Y. Wang, S. Chen, Defects in Graphene: generation, healing, and their effects on the properties of graphene: a Review, J. Mater. Sci. Technol. 31 (2015) 599–606.

[35] R. Ciriminna, N. Zhang, M.-Q. Yang, F. Meneguzzo, Y.-J. Xu, M. Pagliaro, Commercialization of graphene-based technologies: a critical insight, Chem. Commun. 51 (2015) 7090–7095.

[36] A. Ambrosi, C.K. Chua, A. Bonanni, M. Pumera, Electrochemistry of graphene and related materials, Chem. Rev. 114 (2014) 7150–7188.

[37] K. Ullah, A. Ullah, A. Aldalbahi, J. Chung, W.-C. Oh, Enhanced visible light photocatalytic activity and hydrogen evolution through novel heterostructure AgI–FG–TiO2 nanocomposites, J. Mol. Catal. A Chem. 410 (2015) 242–252.

[38] R.Munoz, C.Goìmez-Aleixandre, Review of CVD synthesis of graphene, Chem. Vap. Depos. 19 (2013) 297–322.

[39] D.C. Marcano, D.V. Kosynkin, J.M. Berlin, A. Sinitskii, Z. Sun, A. Slesarev, L.B. Alemany, W. Lu, J.M. Tour, Improved synthesis of graphene oxide, ACS Nano 4 (2010) 4806–4814.

[40] M.J. McAllister, J.-L. Li, D.H. Adamson, H.C. Schniepp, A.A. Abdala, J. Liu, M. Herrera-Alonso, D.L. Milius, R. Car, R.K. Prud'homme, I.A. Aksay, Single sheet functionalized graphene by oxidation and thermal expansion of graphite, Chem. Mater. 19 (2007) 4396–4404.

[41] M. Acik, Y.J. Chabal, A review on thermal exfoliation of graphene oxide, J. Mater. Sci. Res. 2 (2013) 101–112.

[42] V.C. Tung, M.J. Allen, Y. Yang, R.B. Kaner, High-throughput solution processing of large-scale graphene, Nat. Nanotechnol. 4 (2009) 25–29.

[43] K.P. Loh, Q. Bao, G. Eda, M. Chhowalla, Graphene oxide as a chemically tunable platform for optical applications, Nat. Chem. 2 (2010) 1015–1024.

[44] Y. Qiu, F. Guo, R. Hurt, I. Kulaots, Explosive thermal reduction of graphene oxide-based materials: mechanism and safety implications, Carbon 72 (2014) 215–223.

[45] J. Song, X. Wang, C.-T. Chang, Preparation and characterization of graphene oxide, J. Nanomater. 2014 (2014) 1–6.

[46] X. An, J.C. Yu, Graphene-based photocatalytic composites, RSC Adv. 1 (2011) 1426–1434.

[47] N. Zhang, Y. Zhang, Y.-J. Xu, Recent progress on graphene-based photocatalysts: current status and future perspectives, Nanoscale 4 (2012) 5792–5813.

[48] G. Williams, B. Seger, P.V. Kamat, TiO_2 -graphene nanocomposites. UV-assisted photocatalytic reduction of graphene oxide, ACS Nano. 2 (2008) 1487–1491.

[49] C. Xu, J. Zhu, R. Yuan, X. Fu, More effective use of graphene in photocatalysis by conformal attachment of small sheets to TiO_2 spheres, Carbon 96 (2016) 394–402.

[50] A.N. Fouda, E.S.M. Duraia, Self-assembled graphene oxide on a photo-catalytic active transparent conducting oxide, Mater. Des. 90 (2016) 284–290.

[51] C. Liu, L. Zhang, R. Liu, Z. Gao, X. Yang, Z. Tu, F. Yang, Z. Ye, L. Cui, C. Xu, Y. Li, Hydrothermal synthesis of N-doped TiO_2 nanowires and N-doped graphene heterostructures with enhanced photocatalytic properties, J. Alloys Compd. 656 (2016) 24–32

[52] M. Faraji, N. Mohaghegh, Ag/TiO_2-nanotube plates coated with reduced graphene oxide as photocatalysts, Surf. Coat. Technol. 288 (2016) 144–150.

[53] N. Zhang, Y.-J. Xu, The endeavour to advance graphene–semiconductor composite-based photocatalysis, CrystEngComm 18 (2016) 24–37.

[54] S. Cao, T. Liu, Y. Tsang, C. Chen, Role of hydroxylation modification on the structure and property of reduced graphene oxide/TiO_2 hybrids, Appl. Surf. Sci. 382 (2016) 225–238.

[55] N.M. Julkapli, S. Bagheri, Graphene supported heterogeneous catalysts: an overview, Int. J. Hydrogen Energy 40 (2015) 948–979.

[56] T.-F. Yeh, J. Cihlaìr¡, C.-Y. Chang, C. Cheng, H. Teng, Roles of graphene oxide in photocatalytic water splitting, Mater. Today 16 (2013) 78–84.

[57] J. Low, J. Yu, W. Ho, Graphene-based photocatalysts for CO_2 reduction to solar fuel, J. Phys. Chem. Lett. 6 (2015) 4244–4251.

[58] Y. Xu, Y. Mo, J. Tian, P. Wang, H. Yu, J. Yu, The synergistic effect of graphitic N and pyrrolic N for the enhanced photocatalytic performance of nitrogen-doped graphene/TiO2 nanocomposites, Appl. Catal. B 181 (2016) 810–817.

[59] J.T.-W. Wang, J.M. Ball, E.M. Barea, A. Abate, J.A. Alexander-Webber, J. Huang, M. Saliba, I. Mora-Sero, J. Bisquert, H.J. Snaith, R.J. Nicholas, Low-temperature processed electron collection layers of graphene/TiO2 nanocomposites in thin film perovskite solar cells, Nano Lett. 14 (2014) 724–730.

[60] B.Y.S. Chang, M.S. Mehmood, A. Pandikumar, N.M. Huang, H.N. Lim, A.R. Marlinda, N. Yusoff, W.S. Chiu, Hydrothermally prepared graphene-titania nanocomposite for the solar photocatalytic degradation of methylene blue, Desalin. Water Treat. 57 (2015) 238–245.

[61] N. Armaroli, V. Balzani, Solar electricity and solar fuels: status and perspectives in the context of the energy transition, Chem. Eur. J. 22 (2016) 32–57.

[62] R. Long, N.J. English, O.V. Prezhdo, Photo-induced charge separation across the graphene–TiO2 interface is faster than energy losses: a time-domain ab initio analysis, J. Am. Chem. Soc. 134 (2012) 14238–14248.

[63] S. Chowdhury, R. Balasubramanian, Graphene/semiconductor nanocomposites (GSNs) for heterogeneous photocatalytic decolorization of wastewaters contaminated with synthetic dyes: a review, Appl. Catal. B 160 (2014) 307–324.

[64] S. Liu, H. Sun, S. Liu, S. Wang, Graphene facilitated visible light photodegradation of methylene blue over titanium dioxide photocatalysts, Chem. Eng. J. 214 (2013) 298–303.

[65] A. Sharma, B.-K. Lee, Rapid photo-degradation of 2-chlorophenol under visible light irradiation using cobalt oxide-loaded TiO_2 /reduced graphene oxide nanocomposite from aqueous media, J. Environ. Manage. 165 (2016) 1–10.

[66] J. Li, Q. Zhang, L. Zeng, D. He, Synthesis, characterization and photocatalytic study of graphene oxide and cerium co-doped in TiO_2 , Appl. Phys. A 122 (2016) 51.

[67] G. Dai, X. Wang, S. Liu, Y. Liang, K. Liu, Template-free fabrication of hierarchical macro-/mesoporous N-doped TiO_2 /graphene oxide composites with enhanced visible-light photocatalytic activity, J. Chin. Chem. Soc. 62 (2015) 170–176.

[68] M.R. Hasan, S.B. Abd Hamid, W.J. Basirun, Z.Z. Chowdhury, A.E. Kandjani, S.K. Bhargava, Ga doped RGO–TiO_2 composite on an ITO surface electrode for investigation of photoelectrocatalytic activity under visible light irradiation, New J. Chem. 39 (2015) 369–376.

[69] Y. Haldorai, A. Rengaraj, C.H. Kwak, Y.S. Huh, Y.-K. Han, Fabrication of nano TiO_2@graphene composite: reusable photocatalyst for hydrogen production, degradation of organic and inorganic pollutants, Synth. Met. 198 (2014) 10–18.

[70] A.P. Bhirud, S.D. Sathaye, R.P. Waichal, J.D. Ambekar, C.-J. Park, B.B. Kale, In-situ preparation of N-TiO_2 /graphene nanocomposite and its enhanced photocatalytic hydrogen production by H_2S splitting under solar light, Nanoscale 7 (2015) 5023–5034.

[71] H.-H. Chun, W.-K. Jo, Adsorption and photocatalysis of 2-ethyl-1-hexanol over graphene oxide–TiO_2 hybrids post-treated under various thermal conditions, Appl. Catal. B 180 (2016) 740–750.

[72] J. Wei, S. Xue, P. Xie, R. Zou, Synthesis and photocatalytic properties of different SnO2 microspheres on graphene oxide sheets, Appl. Surf. Sci. 376 (2016) 172–179.

[73] D.K. Padhi, G.K. Pradhan, K.M. Parida, S.K. Singh, Facile fabrication of $Gd(OH)_3$ nanorod/RGO composite: synthesis, characterisation and photocatalytic reduction of Cr(VI), Chem. Eng. J. 255 (2014) 78–88.

[74] Y. Wang, Z. Mo, P. Zhang, C. Zhang, L. Han, R. Guo, H. Gou, X. Wei, R. Hu, Synthesis of flower-like TiO_2 microsphere/graphene composite for removal of organic dye from water, Mater. Des. 99 (2016) 378–388.

[75] A. Trapalis, N. Todorova, T. Giannakopoulou, N. Boukos, T. Speliotis, D. Dimotikali, J. Yu, TiO_2 / graphene composite photocatalysts for NOx removal: a comparison of surfactant-stabilized graphene and reduced graphene oxide, Appl. Catal. B 180 (2016) 637–647.

[76] M.S. Sher Shah, K. Zhang, A.R. Park, K.S. Kim, N.-G. Park, J.H. Park, P.J. Yoo, Single-step solvothermal synthesis of mesoporous Ag–TiO_2 –reduced graphene oxide ternary composites with enhanced photocatalytic activity, Nanoscale 5 (2013) 5093–5101.

[77] L. Liu, Z. Liu, A. Liu, X. Gu, C. Ge, F. Gao, L. Dong, Engineering the TiO_2 -graphene interface to enhance photocatalytic H_2 production, ChemSusChem 7 (2014) 618–626.

[78] S. Thangavel, K. Krishnamoorthy, S.-J. Kim, G. Venugopal, Designing ZnS decorated reduced graphene-oxide nanohybrid via microwave route and their application in photocatalysis, J. Alloys Compd. 683 (2016) 456–462.

[79] W. Xiao, Y. Zhang, L. Tian, H. Liu, B. Liu, Y. Pu, Facile synthesis of reduced graphene oxide/titania composite hollow microspheres based on sonication-assisted interfacial self-assembly of tiny graphene oxide sheets and the photocatalytic property, J. Alloys Compd. 665 (2016) 21–30

[80] W.-N. Wang, Y. Jiang, J.D. Fortner, P. Biswas, Nanostructured graphene-titanium dioxide composites synthesized by a single-step aerosol process for photoreduction of carbon dioxide, Environ. Eng. Sci. 31 (2014) 428–434.

[81] B. Luo, G. Liu, L. Wang, Recent advances in 2D materials for photocatalysis, Nanoscale 8 (2016) 6904–6920.

[82] X. Luan, M.T. Gutierrez Wing, Y. Wang, Enhanced photocatalytic activity of graphene oxide/titania nanosheets composites for methylene blue degradation, Mater. Sci. Semicond. Process. 30 (2015) 592–598.

[83] R. Bera, S. Kundu, A. Patra, 2D hybrid nanostructure of reduced graphene oxide-CdS nanosheet for enhanced photocatalysis, ACS Appl. Mater. Interfaces 7 (2015) 13251–13259.

[84] X. Xu, F. Ming, J. Hong, Y. Xie, Z. Wang, Three-dimensional porous aerogel constructed by Bi_2WO_6 nanosheets and graphene with excellent visible-light photocatalytic performance, Mater. Lett. 179 (2016) 52–56.

[85] R. Fang, Y. Liang, X. Ge, M. Du, S. Li, T. Li, Z. Li, Preparation and photocatalytic degradation activity of TiO_2 /rGO/polymer composites, Colloid. Polym. Sci. 293 (2015) 1151–1157.

[86] R. Fang, X. Ge, M. Du, Z. Li, C. Yang, B. Fang, Y. Liang, Preparation of silver/graphene/polymer hybrid microspheres and the study of photocatalytic degradation, Colloid. Polym. Sci. 292 (2014) 985–990.

[87] B. Weng, Y.-J. Xu, What if the electrical conductivity of graphene is significantly deteriorated for the graphene-semiconductor composite-based photocatalysis? ACS Appl. Mater. Interfaces 7 (2015) 27948–27958.

[88] P. MagalhaÞes, J. Angelo, V.M. Sousa, O.C. Nunes, L. Andrade, A. Mendes, Synthesis and assessment of a graphene-based composite photocatalyst, Biochem. Eng. J. 104 (2015) 20–26.

[89] R. Leary, A. Westwood, Carbonaceous nanomaterials for the enhancement of TiO_2 photocatalysis, Carbon 49 (2011) 741–772.

[90] H. Zhang, X. Lv, Y. Li, Y. Wang, J. Li, P25-graphene composite as a high performance photocatalyst,

ACS Nano 4 (2010) 380–386.

[91] H. Wang, T. Maiyalagan, X. Wang, Review on recent progress in nitrogen-doped graphene: synthesis, characterization, and its potential applications, ACS Catal. 2 (2012) 781–794.

[92] S. Sandoval, N. Kumar, A. Sundaresan, C.N.R. Rao, A. Fuertes, G. Tobias, Enhanced thermal oxidation stability of reduced graphene oxide by nitrogen doping, Chem. Eur. J. 20 (2014) 11999–12003.

[93] M. Latorre-Saìnchez, A. Primo, H. Garciìa, P-doped graphene obtained by pyrolysis of modified alginate as a photocatalyst for hydrogen generation from water-methanol mixtures, Angew. Chem. Int. Ed. 52 (2013) 11813–11816.

[94] Y. Zhang, N. Zhang, Z.-R. Tang, Y.-J. Xu, Graphene transforms wide band gap ZnS to a visible light photocatalyst. The new role of graphene as a macromolecular photosensitizer, ACS Nano 6 (2012) 9777–9789.

[95] A.M. Abdelkader, C. Valleìs, A.J. Cooper, I.A. Kinloch, R.A.W. Dryfe, Alkali reduction of graphene oxide in molten halide salts: production of corrugated graphene derivatives for high-performance supercapacitors, ACS Nano 8 (2014) 11225–11233.

[96] J. Hu, H. Li, Q. Wu, Y. Zhao, Q. Jiao, Synthesis of TiO_2 nanowire/reduced graphene oxide nanocomposites and their photocatalytic performances, Chem. Eng. J. 263 (2015) 144–150.

[97] I. Roy, G. Sarkar, S. Mondal, D. Rana, A. Bhattacharyya, N.R. Saha, A. Adhikari, D. Khastgir, S. Chattopadhyay, D. Chattopadhyay, Synthesis and characterization of graphene from waste dry cell battery for electronic applications, RSC Adv. 6 (2016) 10557–10564.

[98] H. Adamu, P. Dubey, J.A. Anderson, Probing the role of thermally reduced graphene oxide in enhancing performance of TiO_2 in photocatalytic phenol removal from aqueous environments, Chem. Eng. J. 284 (2016) 380–388.

[99] N.R. Khalid, E. Ahmed, Z. Hong, Y. Zhang, M. Ahmad, Nitrogen doped TiO_2 nanoparticles decorated on graphene sheets for photocatalysis applications, Curr. Appl. Phys. 12 (2012) 1485–1492.

[100] Y. Chen, G. Tian, G. Mao, R. Li, Y. Xiao, T. Han, Facile synthesis of well-dispersed Bi_2S_3 nanoparticles on reduced graphene oxide and enhanced photocatalytic activity, Appl. Surf. Sci. 378 (2016) 231–238.

[101] H. Gao, W. Chen, J. Yuan, Z. Jiang, G. Hu, W. Shangguan, Y. Sun, J. Su, Controllable O2•-oxidization graphene in TiO_2 /graphene composite and its effect on photocatalytic hydrogen evolution, Int. J. Hydrogen Energy. 38 (2013) 13110–13116.

[102] F. Wang, M. Zheng, C. Zhu, B. Zhang, W. Chen, L. Ma, W. Shen, Visible light photocatalytic H_2 -production activity of wide band gap ZnS nanoparticles based on the photosensitization of graphene, Nanotechnology 26 (2015) 345–402.

[103] M.E. Khan, M.M. Khan, M.H. Cho, Biogenic synthesis of a Ag-graphene nanocomposite with efficient photocatalytic degradation, electrical conductivity and photoelectrochemical performance, New J. Chem. 39 (2015) 8121–8129.

[104] J. Chen, J. Shi, X. Wang, H. Cui, M. Fu, Recent progress in the preparation and application of semiconductor/graphene composite photocatalysts, Chin. J. Catal. 34 (2013) 621–640

[105] X. An, K. Li, J. Tang, Cu_2O/reduced graphene oxide composites for the photocatalytic conversion of CO_2 , ChemSusChem 7 (2014) 1086–1093.

[106] Z. Ren, E. Kim, S.W. Pattinson, K.S. Subrahmanyam, C.N.R. Rao, A.K. Cheetham, D. Eder, Hybridizing photoactive zeolites with graphene: a powerful strategy towards superior photocatalytic properties, Chem. Sci. 3 (2012) 209–216.

[107] M. Minella, F. Sordello, C. Minero, Photocatalytic process in TiO_2 /graphene hybrid materials. Evidence of charge separation by electron transfer from reduced graphene oxide to TiO_2 , Catal. Today 281 (2017) 29–37.

[108] P. Wang, J. Wang, X. Wang, H. Yu, J. Yu, M. Lei, Y. Wang, One-step synthesis of easy-recycling TiO_2-rGO nanocomposite photocatalysts with enhanced photocatalytic activity, Appl. Catal. B 132 (2013)

452–459.

[109] L.M. Pastrana-Martiìnez, S. Morales-Torres, V. Likodimos, J.L. Figueiredo, J.L. Faria, P. Falaras, A.M.T. Silva, Advanced nanostructured photocatalysts based on reduced graphene oxide–TiO_2 composites for degradation of diphenhydramine pharmaceutical and methyl orange dye, Appl. Catal. B 123–124 (2012) 241–256.

[110] D.S. Bhatkhande, V.G. Pangarkar, A.A.C.M. Beenackers, Photocatalytic degradation for environmental applications – a review, J. Chem. Technol. Biotechnol. 77 (2002) 102–116.

[111] L. Wang, M. Wen, W. Wang, N. Momuinou, Z. Wang, S. Li, Photocatalytic degradation of organic pollutants using rGO supported TiO_2-CdS composite undervisiblelightirradiation, J.AlloysCompd.683(2016)318–328.

[112] F. Perreault, A. Fonseca de Faria, M. Elimelech, Environmental applications of graphene-based nanomaterials, Chem. Soc. Rev. 44 (2015) 5861–5896.

[113] C.-C. Wang, X.-D. Du, J. Li, X.-X. Guo, P. Wang, J. Zhang, Photocatalytic Cr(VI) reduction in metal-organic frameworks: a mini-review, Appl. Catal. B 193 (2016) 198–216.

[114] Q. Xiang, J. Yu, M. Jaroniec, Graphene-based semiconductor photocatalysts, Chem. Soc. Rev. 41 (2012) 782–796.

[115] L.M. Pastrana-Martiìnez, S. Morales-Torres, V. Likodimos, P. Falaras, J.L. Figueiredo, J.L. Faria, A.M.T. Silva, Role of oxygen functionalities on the synthesis of photocatalytically active graphene–TiO_2 composites, Appl. Catal. B 158-159 (2014) 329–340.

[116] A. Ahmad, S.H. Mohd-Setapar, C.S. Chuong, A. Khatoon, W.A. Wani, R. Kumar, M. Rafatullah, Recent advances in new generation dye removal technologies: novel search for approaches to reprocess wastewater, RSC Adv. 5 (2015) 30801–30818.

[117] M.E. Khan, M.M. Khan, M.H. Cho, CdS-graphene nanocomposite for efficient visible-light-driven photocatalytic and photoelectrochemical applications, J. Colloid Interface Sci. 482 (2016) 221–232.

[118] M. Faraji, N. Mohaghegh, Ag/TiO_2 -nanotube plates coated with reduced graphene oxide as photocatalysts, Surf. Coat. Technol. 288 (2016) 144–150.

[119] K. Li, T. Chen, L. Yan, Y. Dai, Z. Huang, J. Xiong, D. Song, Y. Lv, Z. Zeng, Design of graphene and silica co-doped titania composites with ordered mesostructure and their simulated sunlight photocatalytic performance towards atrazine degradation, Colloids Surf. A Physicochem. Eng. Asp. 422 (2013) 90–99.

[120] N. Prabhakarrao, M.R. Chandra, T.S. Rao, Synthesis of Zr doped TiO_2 /reduced Graphene Oxide (rGO) nanocomposite material for efficient photocatalytic degradation of Eosin Blue dye under visible light irradiation, J. Alloys Compd. 694 (2017) 596–606.

[121] R.K. Upadhyay, N. Soin, S.S. Roy, Role of graphene/metal oxide composites as photocatalysts, adsorbents and disinfectants in water treatment: a review, RSC Adv. 4 (2014) 3823–3851.

[122] M. Mukthar Ali, K.Y. Sandhya, Selective photodegradation and enhanced photo electrochemical properties of titanium dioxide-graphene composite with exposed (001) facets made by photochemical method, Sol. Energy Mater. Sol. Cells 144 (2016) 748–757.

[123] Y. Yang, L. Xu, H. Wang, W. Wang, L. Zhang, TiO_2 /graphene porous composite and its photocatalytic degradation of methylene blue, Mater. Des. 108 (2016) 632–639.

[124] L. Liu, C. Luo, J. Xiong, Z. Yang, Y. Zhang, Y. Cai, H. Gu, Reduced graphene oxide (rGO) decorated TiO2 microspheres for visible-light photocatalytic reduction of Cr(VI), J. Alloys Compd. 690 (2017) 771–776.

[125] Y. Li, W. Cui, L. Liu, R. Zong, W. Yao, Y. Liang, Y. Zhu, Removal of Cr(VI) by 3D TiO_2 -graphene hydrogel via adsorption enriched with photocatalytic reduction, Appl. Catal. B 199 (2016) 412–423.

[126] L. Wang, M. Wen, W. Wang, N. Momuinou, Z. Wang, S. Li, Photocatalytic degradation of organic pollutants using rGO supported TiO_2 -CdS composite under visible light irradiation, J. Alloys Compd.

683 (2016) 318–328.

[127] Y. Ding, Y. Zhou, W. Nie, P. Chen, MoS_2 –GO nanocomposites synthesized via a hydrothermal hydrogel method for solar light photocatalytic degradation of methylene blue, Appl. Surf. Sci. 357 (2015) 1606–1612.

[128] L. Gan, L. Xu, S. Shang, X. Zhou, L. Meng, Visible light induced methylene blue dye degradation photo-catalyzed by WO_3 /graphene nanocomposites and the mechanism, Ceram. Int. 42 (2016) 15235–15241.

[129] J. Qin, X. Zhang, C. Yang, M. Cao, M. Ma, R. Liu, ZnO microspheres-reduced graphene oxide nanocomposite for photocatalytic degradation of methylene blue dye, Appl. Surf. Sci. 392 (2017) 196–203.

[130] S. Kumar, A.K. Ojha, B. Walkenfort, Cadmium oxide nanoparticles grown in situ on reduced graphene oxide for enhanced photocatalytic degradation of methylene blue dye under ultraviolet irradiation, J. Photochem. Photobiol. B 159 (2016) 111–119.

[131] P.K. Boruah, P. Borthakur, G. Darabdhara, C.K. Kamaja, I. Karbhal, M.V. Shelke, P. Phukan, D. Saikia, M.R. Das, Sunlight assisted degradation of dye molecules and reduction of toxic Cr(VI) in aqueous medium using magnetically recoverable Fe_3O_4 /reduced graphene oxide nanocomposite, RSC Adv. 6 (2016) 11049–11063.

[132] J. Li, L. Zheng, L. Li, Y. Xian, L. Jin, Fabrication of TiO_2 /Ti electrode by laser-assisted anodic oxidation and its application on photoelectrocatalytic degradation of methylene blue, J. Hazard. Mater. 139 (2007) 72–78.

[133] F. Zhang, M. Chen, W. Oh, Photoelectrocatalytic properties of Ag-CNT/TiO_2 composite electrodes for methylene blue degradation, New Carbon Mater. 25 (2010) 348–356.

[134] W. Han, L. Ren, Z. Zhang, X. Qi, Y. Liu, Z. Huang, J. Zhong, Graphene-supported flocculent-like TiO_2 nanostructures for enhanced photoelectrochemical activity and photodegradation performance, Ceram. Int. 41 (2015) 7471–7477.

[135] F. Han, H. Li, J. Yang, X. Cai, L. Fu, One-pot synthesis of cuprous oxide-reduced graphene oxide nanocomposite with enhanced photocatalytic and electrocatalytic performance, Phys. E 77 (2016) 122–126.

[136] T. An, W. Zhang, X. Xiao, G. Sheng, J. Fu, X. Zhu, Photoelectrocatalytic degradation of quinoline with a novel three-dimensional electrode-packed bed photocatalytic reactor, J. Photochem. Photobiol. A 161 (2004) 233–242.

[137] X.Z. Li, C. He, N. Graham, Y. Xiong, Photoelectrocatalytic degradation of bisphenol A in aqueous solution using a Au–TiO_2 /ITO film, J. Appl. Electrochem. 35 (2005) 741–750.

[138] Q. Zhou, A. Xing, J. Li, D. Zhao, K. Zhao, M. Lei, Synergistic enhancement in photoelectrocatalytic degradation of bisphenol A by CeO_2 and reduced graphene oxide co-modified TiO_2 nanotube arrays in combination with Fenton oxidation, Electrochim. Acta 209 (2016) 379–388.

[139] B. Zhu, B. Lin, Y. Zhou, P. Sun, Q. Yao, Y. Chen, B. Gao, Enhanced photocatalytic H_2 evolution on ZnS loaded with graphene and MoS_2 nanosheets as cocatalysts, J. Mater. Chem. A 2 (2014) 3819–3827.

[140] Z. Yan, X. Yu, A. Han, P. Xu, P. Du, Noble-metal-free $Ni(OH)_2$ -modified CdS/reduced graphene oxide nanocomposite with enhanced photocatalytic activity for hydrogen production under visible light irradiation, J. Phys. Chem. C. 118 (2014) 22896–22903.

[141] P. Gao, D.D. Sun, Hierarchical sulfonated graphene oxide–TiO_2 composites for highly efficient hydrogen production with a wide pH range, Appl. Catal. B 147 (2014) 888–896.

[142] W. Han, L. Ren, X. Qi, Y. Liu, X. Wei, Z. Huang, J. Zhong, Synthesis of CdS/ZnO/graphene composite with high-efficiency photoelectrochemical activities under solar radiation, Appl. Surf. Sci. 299 (2014) 12–18.

[143] M.A. Fox, Organic heterogeneous photocatalysis: chemical conversions sensitized by irradiated

semiconductors, Acc. Chem. Res. 16 (1983) 314–321.

[144] G. Palmisano, V. Augugliaro, M. Pagliaro, L. Palmisano, Photocatalysis: a promising route for 21 st century organic chemistry, Chem. Commun. 95 (2007) 3425–3437.

[145] D. Friedmann, A. Hakki, H. Kim, W. Choi, D. Bahnemann, Heterogeneous photocatalytic organic synthesis: state-of-the-art and future perspectives, Green Chem. 18 (2016) 5391–5411.

[146] J. Yang, X. Shen, Y. Li, L. Bian, J. Dai, D. Yuan, Bismuth tungstate-reduced graphene oxide self-assembled nanocomposites for the selective photocatalytic oxidation of alcohols in water, ChemCatChem 8 (2016) 1399–1409.

[147] J. Xu, S. He, H. Zhang, J. Huang, H. Lin, X. Wang, J. Long, Layered metal-organic framework/graphene nanoarchitectures for organic photosynthesis under visible light, J. Mater. Chem. A 3 (2015) 24261–24271.

[148] T. Inoue, A. Fujishima, S. Konishi, K. Honda, Photoelectrocatalytic reduction of carbon dioxide in aqueous suspensions of semiconductor powders, Nature 277 (1979) 637–638.

[149] Y.T. Liang, B.K. Vijayan, O. Lyandres, K.A. Gray, M.C. Hersam, Effect of dimensionality on the photocatalytic behavior of carbon-titania nanosheet composites: charge transfer at nanomaterial interfaces, J. Phys. Chem. Lett. 3 (2012) 1760–1765.

[150] M.R. Hasan, S.B. Abd Hamid, W.J. Basirun, Charge transfer behavior of graphene-titania photoanode in CO_2 photoelectrocatalysis process, Appl. Surf. Sci. 339 (2015) 22–27.

[151] K.S. Novoselov, V.I. Fal'ko, L. Colombo, P.R. Gellert, M.G. Schwab, K. Kim, A roadmap for graphene, Nature 490 (2012) 192–200.

[152] M.R. Hasan, S.B. Abd Hamid, W.J. Basirun, S.H. Meriam Suhaimy, A.N. Che Mat, A sol–gel derived, copper-doped, titanium dioxide–reduced graphene oxide nanocomposite electrode for the photoelectrocatalytic reduction of CO_2 to methanol and formic acid, RSC Adv. 5 (2015) 77803–77813.

[153] Q. Li, W. Zhu, J. Fu, H. Zhang, G. Wu, S. Sun, Controlled assembly of Cu nanoparticles on pyridinic-N rich graphene for electrochemical reduction of CO_2 to ethylene, Nano Energy 24 (2016) 1–9.

[154] Y. Xia, S. Pezzini, E. Treossi, G. Giambastiani, F. Corticelli, V. Morandi, A. Zanelli, V. Bellani, V. Palermo, The exfoliation of graphene in liquids by electrochemical, chemical, and sonication-assisted techniques: a nanoscale study, Adv. Funct. Mater. 23 (2013) 4684–4693.

[155] I.-H. Tseng, W.-C. Chang, J.C.S. Wu, Photoreduction of CO_2 using sol–gel derived titania and titania-supported copper catalysts, Appl. Catal. B 37 (2002) 37–48.

[156] W. Tu, Y. Zhou, Q. Liu, S. Yan, S. Bao, X. Wang, M. Xiao, Z. Zou, An in situ simultaneous reduction-hydrolysis technique for fabrication of TiO_2 -graphene 2D sandwich-like hybrid nanosheets: graphene-promoted selectivity of photocatalytic-driven hydrogenation and coupling of CO_2 into methane and ethane, Adv. Funct. Mater. 23 (2013) 1743–1749.